SUBMITTED

Climate scientists may misrepresent future flood risks using popular extreme sea level metrics

D.J. Rasmussen, Scott Kulp, Robert E. Kopp, Michael Oppenheimer, and Benjamin H. Strauss

Draft: October 2, 2020

Abstract Estimating changes in the frequency or height of extreme sea levels (ESLs; e.g., the 100-yr event) is a popular approach used by climate and sea level scientists to communicate future coastal flood risk to policy makers and the public under various climate change scenarios. However, physical ESL metrics and associated thresholds only account for water levels (i.e., the hazard). They do not consider societal outcomes (e.g., loss of life, property damage). As a result, policy makers may inadvertently disseminate misleading estimates of future coastal flood risk under different climate scenarios. This has critical implications for risk communication and adaptation decision-making. Here, we illustrate how some measures of societal exposure can lead to sizable differences in estimates of future coastal flood risk, relative to when only considering physical impacts using 1) projected ESLs under +2 °C and +5 °C temperature stabilization scenarios and 2) the current population exposure of 414 cities around the world. For some locations with a modest projected increase in the height of an ESL event, the corresponding change in local population exposure is substantial. This suggests that physical ESL metrics may be poor surrogates for capturing some societal impacts. While population exposure is just one measure, communicating a variety of human system, natural resource, and ecosystem-based outcomes may provide a more complete snapshot of either exposure or coastal flood risk under a wide array of climate scenarios.

1 Introduction

Extreme sea levels (ESLs) are the occurrence or the level of a short-lived (hours to days), exceptionally high local sea-surface height, usually as a result of coastal storms, waves, or astronomical tides (Gregory et al, 2019). When ESLs overtop natural (e.g., dunes, cliffs) or engineered (e.g., seawalls, bulkheads, levees) protection, potentially deadly and costly floods can occur in areas unprepared to deal with the hazard. Observational studies have shown that ESLs are occurring at tide gauges with increasing frequency, largely as a result of rising mean sea level (MSL) due to global warming and other non-climatic local factors (e.g., ground subsidence; Sweet and Park, 2014; Dahl et al, 2017; Menéndez and Woodworth, 2010). State-of-the-art global flood exposure assessments that consider future projections of sea level change, inundation from ESLs, and current distributions of populations and property have estimated that hundreds of millions of people and trillions of U.S dollars in property value are susceptible (Neumann et al, 2015; Kirezci et al, 2020; Hanson et al, 2011; Kulp and Strauss, 2019; McGranahan et al, 2007; Jongman et al, 2012; Lichter et al, 2011). Global

D.J. Rasmussen
Princeton School of Public & International Affairs, Princeton University, Princeton, NJ, USA. E-mail: dj.rasmussen@princeton.edu

Scott Kulp and Benjamin H. Strauss
Climate Central, Princeton, NJ, USA

Robert E. Kopp
Department of Earth & Planetary Sciences, Rutgers Energy Institute, and Institute of Earth, Ocean, & Atmospheric Sciences, Rutgers University, New Brunswick, NJ, USA.

Michael Oppenheimer
Department of Geosciences and Princeton School of Public & International Affairs, Princeton University, Princeton, NJ, USA.

flood risk assessments (risk as defined by Weyer, In press) that consider the interaction of hazard, exposure, and vulnerability have found that ESLs are projected to cost trillions of U.S. dollars per year by 2100 (Diaz, 2016; Hinkel et al, 2014; Jevrejeva et al, 2018). While these studies are essential for broadly communicating climate risks, they generally only consider a few sea level scenarios, which is insufficient to account for the true state of uncertainty in future sea level change (Kopp et al, 2019b). On the other hand, ESL frequency amplification factors (AFs) developed by climate and sea level scientists are relatively simple calculations that can be run on a desktop computer to quickly estimate changes in still water level hazards at a tide gauge under a wide array of future sea level projections.

ESL frequency AFs (also called "factors of increase" or "multiplication factors") indicate the change in the expected frequency of a given ESL event (e.g., the 1-in-100-yr ESL event; Hunter, 2012; Buchanan et al, 2017; Rasmussen et al, 2018; Frederikse et al, 2020; Vitousek et al, 2017; Taherkhani et al, 2020; Church et al, 2013; Howard and Palmer, 2020). For example, a 0.5 m increase in MSL at a tide gauge in San Juan, Puerto Rico is expected to increase the frequency of the historical 100-yr ESL event from 0.01 events yr^{-1} to ∼30 events yr^{-1}, on average (i.e., an AF of 3000; Rasmussen et al, 2018). Similarly, ESL return level AFs denote the relative change in the height of the ESL associated with a given return period. Both ESL frequency and return level AFs have often been used by climate scientists to communicate "flood risk" to policy makers and the public under a wide array of future sea level scenarios (Vitousek et al, 2017; Taherkhani et al, 2020; Buchanan et al, 2017; Kriebel et al, 2015; Frederikse et al, 2020; Garner et al, 2017; Howard and Palmer, 2020), including multiple plausible contributions from "deeply uncertain"[1] sea level components, such as the Antarctic Ice Sheet (Rasmussen et al, 2020; Frederikse et al, 2020).

While ESL frequency AFs purport to communicate "flood risk" , they only consider still water height at a tide gauge (i.e., the hazard), such as the height of the 100-yr ESL event. They do not consider the corresponding level of exposure (e.g., population or damage to property and natural resources), nor do they consider vulnerability. This is important because ESL AFs have appeared in prominent climate assessment reports such as the Intergovernmental Panel on Climate Change (IPCC)(Oppenheimer et al, in press; Wong et al, 2014; Church et al, 2013), the U.S. National Climate Assessment (Sweet et al, 2017), and others (Kopp et al, 2019a). Without a proper distinction, climate scientists and policy makers could disseminate misleading projections of coastal flood risk. For example, investigators that have focused on the frequency of exceedances of physical thresholds (e.g., the height of the 50-yr ESL event) have claimed that 0.5 m of MSL rise could lead to a doubling of "flood" events within decades for certain regions (Vitousek et al, 2017) or exponential increases in the frequency of "floods" (quotes imply authors mean ESLs; Taherkhani et al, 2020). While these claims may be true of the hazard (i.e., ESLs), they may not apply to the corresponding societal outcome (e.g., "a doubling of population exposure" or an "exponential increase in the rate of population exposure"). Some locations may be protected to a level above the height of the ESL event in question (i.e., no flood occurs), or there may exist little to no societal exposure at or below the ESL height (i.e., a flood occurs, but there is no societal impact). In the San Juan example, while the historical 100-yr ESL event is projected to occur ∼3000 times as often under a 0.5 m increase in MSL, there are currently $<$ 1,000 people living below the elevation of the 100-ESL event ($<$ 0.1% of the total city population; Fig. 1). Hauer et al (2020) also recently noted differences between projections of physical ESL metrics and those that are based on population exposure in the U.S.

The problems associated with metrics omitting exposure and vulnerability extend beyond risk communication. Climate and sea level scientists have also developed frameworks intended to optimize the design of coastal risk reduction strategies that only consider the return periods of still water heights. For example, ESL hazard "allowances" have been developed to assist flood managers seeking to maintain a given level of flood protection under uncertain sea level change (Howard and Palmer, 2020; Hunter, 2012; Hunter et al, 2013; Buchanan et al, 2016; Slangen et al, 2017). A hazard allowance is a deliberately-selected vertical buffer intended to ensure that the expected number of ESL events is kept constant as sea levels change (e.g., the height of a levee that protects against the 100-yr ESL event). These events are usually measured at tide gauges, which may differ from the return period of floods at other inland locations (Moore and Obradovich, 2020).

[1] Deep uncertainty (also synonymous with Knightian uncertainty and Ellsbergian 'ambiguity') describes situations where there is either ignorance or disagreement by experts or decision makers over 1) conceptual models used to describe key system processes and 2) probability distribution functions used to characterize uncertainty related to key variables and parameters (Weyer, In press)

Without inundation modeling, ESL hazard allowances calculated at tide gauges may lead to sub-optimal flood protection designs (e.g., Rasmussen et al, 2020).

In this study, we use a simple inundation model with a new global elevation dataset (Kulp and Strauss, 2018, 2019) to highlight the limitations and consequences of using ESL metrics that only consider the physical heights of water levels, specifically ESL AFs (frequency and return level) and ESL hazard allowances. We connect ESLs measured at a global network of tide gauges to present-day population exposure for 414 coastal cities around the world. We project future changes in both the frequency and return levels of historical ESLs and the exposure of current populations under two climate change scenarios (Sec. 3.1). We note that these are not estimates of future population exposure because we do not make future projections of population change. Additionally, we use a simple, static inundation approach that has not been globally validated. These projections are merely intended to highlight the limitations of physical ESL metrics when quantifying coastal flood risk. Sophisticated flood risk analyses are needed to better understand current and future risk levels. We then show how ESL hazard allowances may under-predict the necessary vertical buffer needed to maintain a hypothetical exposure-based protection level (Sec. 3.2). While population exposure is used as the risk measure in this study, it is just one component of coastal flood risk, broadly speaking. A diversity of possible metrics exist. We illustrate how using other risk measures could capture other relevant components of the same "coastal risk story" (Sec. 3.3). This includes impacts to vulnerable demographics, property damage, critical infrastructure, loss of natural resources, and harm to ecosystem services (e.g., wetland loss). Future studies could use our framework to further explore these metrics using other datasets.

2 Framework

An overview of the sources of information used to generate population inundation estimates are given in Fig. S-1. Additional details and limitations to our approach are given in the supporting information (Secs. S-1.1 to 2.4). First, we estimate the present-day probability of ESLs of various heights at a global network of tide gauges using extreme value theory and a long-term record of hourly sea level observations (Sec. S-1.1). Second, we project changes in both the frequency and height of ESLs using local probabilistic projections of relative sea level change (RSLC)[2] that incorporate ice sheet mass loss estimates from structured expert judgment (Sec. 2.1). Third, we produce 1-dimensional, city-specific functions of population versus ground elevation to estimate the current population exposure to ESLs (Sec. 2.2). Fourth, by combining the population exposure damage functions with the future estimates of ESLs, we compute the change in the number of people exposed to various ESLs for each city using population exposure AFs (Sec. 2.3). Finally, we use ESL allowances to calculate the vertical buffer needed to maintain the current expected annual population exposure (Sec. 2.4).

2.1 Relative sea level change projections

Probabilistic, time-varying, local RSLC projections for each tide gauge are taken from the component-based study of Kopp et al (2014), except that ice sheet contributions are from the structured expert judgement (SEJ) study of Bamber et al (2019). Projections of RSLC after mid-century are highly dependent on ice sheet melt because of their potential for substantial contributions to global mean sea-level rise (Oppenheimer et al, in press; Kopp et al, 2019b). However, incomplete understanding of the physical processes that govern ice sheet melt inhibits realistic representations in process-based models. In such cases of incomplete scientific understanding, SEJ using calibrated expert responses is one approach for estimating such uncertain quantities (as employed here). Each RSLC probability distribution is conditional on a scenario in which global mean surface air temperature (GSAT) stabilizes in 2100 at either +2 °C (consistent with the Paris Agreement; UNFCCC, 2015) or +5 °C (consistent with unchecked emissions growth; GSAT relative to 1850–1900; Hausfather and Peters, 2020). Samples from each RSLC probability distribution are used to shift the ESL return curves in the direction of the RSLC. Figs. 2A and 2D show the future (2070) ESL return curves for tide gauges located at San Juan (Puerto Rico) and Sewell's Point (Norfolk, USA). The "kinks" in the return curves appear as a result of the highest samples in the RSLC probability distribution causing the expected

[2] Relative sea level change is defined as the change in local mean sea level relative to the sea floor or the underwater surface of the solid Earth (Gregory et al, 2019).

ESL frequency calculation to saturate and then subsequently increase the expected number of ESL events. Both the positioning and the presence of the kinks are sensitive to the choice of where the upper-tail of the RSLC distribution is truncated (Rasmussen et al, 2020). More details and limitations are provided in the supporting information (Sec. S-1.2).

2.2 Exposure analysis

We map flood extents for each city using the "bathtub" model, a static inundation approach that only considers the vertical elevation of two surfaces, 1) the terrain and 2) a given ESL return level (e.g., 100-yr event) measured at the nearest tide gauge within a 100-km radius of each city center. The return level of interest is spatially extrapolated over the terrain. Static inundation approaches have many limitations (Sec. S-1.3), including overestimating observed flood extents relative to hydrodynamic models (Breilh et al, 2013; Gallien, 2016; Ramirez et al, 2016; Seenath et al, 2016; Bates et al, 2005; Vousdoukas et al, 2016). However, hydrodynamic modeling is computationally expensive, and producing state-of-the-art projections of population exposure is not the goal of this study. Land elevation data are from CoastalDEM, a modified version of NASA's Shuttle Radar Topography Mission (SRTM) digital elevation model (DEM) that uses a neural network trained using lidar-derived elevation data in the U.S. (NOAA, 2020) to reduce SRTM errors (Kulp and Strauss, 2018, 2019; Farr et al, 2007). The SRTM is a near-global DEM commonly used for flood exposure modeling but is known to have large vertical bias (an estimated 3.7 m in coastal areas in the U.S.; Kulp and Strauss, 2018). This is important because coastal flood risk analysis is largely performed within this elevation range and these biases are roughly the same magnitude as projections of future local RSLC over this century (generally < 2 m relative to 2000; Oppenheimer et al, in press). More details and limitations are provided in both the supporting information (Sec. S-1.3) and in Kulp and Strauss (2018, 2019).

The vertical population profile of a city can determine the population exposure to a given ESL event. We produce 1-dimensional (vertical) population profiles for 414 global cities using CoastalDEM and population density data from the WorldPop 2010 high resolution (3 arc second) gridded global population data set (Tatem, 2017). In order to simplify our analysis and also isolate the impact of RSLC on population exposure, we assume that population remains fixed in time. Thus, our results are not literal projections of future population exposure—which will depend upon population growth (Hauer et al, 2016; Jongman et al, 2012) and the dynamic response of the population to RSLC (Merkens et al, 2016; Hauer, 2017)—but are instead intended to highlight the impact of ESL events relative to changes in their frequency. Population exposure profiles for San Juan (Puerto Rico) and Norfolk (USA) are given in Figs. 2B,E. Exposure profiles for all cities are included in the supporting data.

Most populations living in low-lying areas around the world (e.g., deltaic regions) are very likely protected by flood defenses such as levees, seawalls, and deliberately raised structures (e.g., buildings on stilts; Scussolini et al, 2016). Following previous flood exposure studies (Neumann et al, 2015; Hanson et al, 2011; Kulp and Strauss, 2019; McGranahan et al, 2007; Jongman et al, 2012; Lichter et al, 2011), our exposure estimates do not account for these defenses because they can be overtopped and breached; only the population in the floodplain is considered. However, protection is assumed to only change the flood hazard and enters our integrated calculations of population exposure that consider all ESL return levels (Sec. 2.4). To our knowledge, verified, location-specific levels of protection are not available at the global scale[3]. To account for flood defenses that provide a margin of safety, we make multiple arbitrary assumptions regarding the current level of protection for all cities. Specifically, we produce results assuming spatially uniform "no protection" and protection up to the height of the 1- and 10-yr ESL event. These assumptions may greatly differ from reality and could lead to gross over-estimates for cities with existing flood protection that afford a high margin of safety from rare storms, such as London, New Orleans, Tokyo, Shanghai, and most major cities in the Netherlands (Nicholls et al, 2008; Hallegatte et al, 2013; Xian et al, 2018; Scussolini et al, 2016). Despite this, we still include protection assumptions for all cities to 1) limit the inclusion of the lowest elevations which are most prone to vertical errors in the DEM (Sec. S-1.3) and 2) to highlight the importance of the flood protection assumption and the need for accurate estimates thereof (e.g., Scussolini et al, 2016).

[3] However, Hallegatte et al (2013) and Scussolini et al (2016) give upper and lower estimates of flood protection for over 100 major cities around the world based on surveyed responses from local experts. But these responses have not been verified, and local protection can vary within a city.

2.3 Estimating physical and population exposure amplification factors

Following Buchanan et al (2017), the ESL frequency AF for an event of height z^* under uncertain RSLC is $\mathbb{E}[N(z^* - \delta)/N(z^*)]$, where $N(z^* - \delta)$ is the expected number of exceedances of height z^* after considering RSLC δ (Sec. S-1.1). The ESL return level AF is given by $1 + \mathbb{E}[\delta]/z^*$. Here, we extend the ESL return level AF to changes in population exposure. We define the population exposure AF for an event of height z^* under uncertain RSLC as $\mathbb{E}[D(z^* + \delta)/D(z^*)]$, where $D(\cdot)$ is a 1-dimensional vertical population profile of a city (Sec. 2.2). Note that since $D(\cdot)$ is solely a function of z, the frequency amplification of population exposure events is equivalent to the ESL frequency AFs for the same city. Probability distributions of ESL AFs (frequency and return level) and population exposure AFs are produced for each tide gauge using the RSLC samples for each climate scenario (Sec. 2.1). Results are then taken from these distributions (Sec. 3).

2.4 Estimating population exposure allowances

While population exposure AFs are well suited to identify and communicate future societal impacts at local scales, ESL allowances are instead intended to optimize the design height of flood protection when desiring to maintain a specific margin of safety under uncertain sea level change (as opposed to using a benefit-cost approach). Expressed mathematically, if $f(z^*)$ is the current annual exceedance probability (AEP) with return level z^* (e.g., the 100-yr event), then the ESL hazard allowance $A(z^*)$ that maintains the current AEP under uncertain sea level change Δ is given by:

$$f(z^*) = \int_{\Delta} f(z^* - \Delta + A(z^*))P(\Delta)\,\mathrm{d}\Delta, \tag{1}$$

where $f(z^* - \Delta)$ is the AEP of z^* after including sea level change Δ whose uncertainty is given by the PDF, $P(\Delta)$. If Δ is known, then $A = \Delta$. Rasmussen et al (2020) extended ESL hazard allowances to facilitate optimizing the height of a flood mitigation strategy (e.g., elevation of structures, levee height, necessary coastal retreat) needed to maintain a given region's historical annual average loss (i.e., a "damage" allowance). Damage allowances conceptually illustrate the consequences of including aspects of exposure and vulnerability when designing adaptive solutions. In lieu of damages, here we consider the expected annual population exposure (EAE) to illustrate the limitations of hazard allowances. An overview of both sea level allowances and the EAE is given in the SI (Sec. S-1.4).

To offset additional population exposure due to RSLC, we create a "protected" population exposure function using an idealized representation of how a flood reduction strategy could impact the relationship between ESLs and populations affected by floods. Specifically, we assume that the city population elevates by an amount A. This corresponds to a horizontal shift of the unprotected populated exposure function $D(z)$ (Sec. 2.2). This strategy is purely hypothetical and is only intended to illustrate differences between allowance frameworks that both do and do not consider societal exposure. In order to maintain the historical EAE under uncertain RSLC, the current EAE must equal the projected EAE that includes both an arbitrary sea level change (δ) and the adjustment A to offset the change in EAE resulting from RSLC. This can be mathematically represented by:

$$\int_{A_{min}}^{\infty} \int_{\delta} D(z - A)f(z - \delta)P(\delta)\,\mathrm{d}\delta\,\mathrm{d}z = \int_{A_{min}}^{\infty} D(z)f(z)\,\mathrm{d}z, \tag{2}$$

where $D(z - A)$ is a protected populated exposure function that elevates all populations within the damage function by the height A such that the current EAE is maintained under RSLC and A_{min} is the height of the assumed current protection level (either no protection, the height of the 1-ESL event or the 10-yr ESL event; Sec. 2.2).

3 Results

3.1 Extreme sea level metrics may poorly predict population exposure

We highlight two cities to illustrate how a policy maker could both over- and under-estimate coastal flood exposure using a physical ESL metric. In San Juan (Puerto Rico), by 2070 the expected frequency of the historical 100-yr ESL event increases from 0.01/yr to a noteworthy 30/yr (+2 °C) and 102/yr (+5 °C), on average (Tables 1,2; Fig. 2A). However, < 1,000 people (< 0.1% of the total population) are currently exposed to the historical 100-yr ESL event (Figs. 1C and 2B,C). While sea-level rise is expected to increase the height of the 100-yr ESL event from 0.7 m above MHHW to 1.2 m (+2 °C) and 1.4 m (+5 °C), the corresponding population exposure is still < 0.1% of the total population (Tables 1,2; Figs. 2B,C). This is due to a low gradient in the population profile over the range of increase in the return level, partially as a result of a steep shoreline around much of San Juan (Figs. 1A and 2B). On the other hand, Norfolk (USA) has both a much steeper population profile than San Juan over the range of increase in the expected 100-yr return level (Fig. 2E) and a greater fraction of its total current population is exposed to the 100-yr ESL event (2.3%; Tables 1,2). By 2070, the expected 100-yr ESL return level increases from 1.5 m above MHHW to 2.1 m (+2 °C) and 2.4 m (+5 °C). This increases the expected population exposure to the 100-yr ESL from ∼16,000 to 64,000 (+2 °C) and 104,000 (+5 °C; Tables 1,2; Figs. 2E,F). Results for an additional 17 other cities and their uncertainties are given in Tables 1,2.

Relationships between physical and societal metrics vary by city in part due to differences in RSLC and the shape of both the ESL return curves and population profiles (Fig. S-2). Globally, population exposure AFs vary from < 1 to > 10 (Fig. 3A). We sort global cities by geographic region in order to look for more localized patterns (Fig. 3B; the region/city mapping is given in the supporting data files). Across most regions examined, ESL return level AFs generally underestimate risks related to population exposure. Notable exceptions are the western coasts of North America and South America. Within these regions, there is a greater fraction of cities with a stronger correlation between ESL return level AFs and population exposure AFs. This suggests that population profiles are more linear over the range of increases in the height of the 100-yr ESL, perhaps due to a smaller variance in ESLs as a result of 1) a narrower continental shelf that leads to a smaller tidal range (Pugh and Woodworth, 2014) and 2) fewer tropical cyclones (Knapp et al, 2010). Plots for 2100 and for the +5 °C scenario are given in the supporting information and results for all cities are tabulated in the supporting data files.

The 100-yr ESL is just one of many possible hazards. Integrated metrics, like the EAE (Section 2.4), considers the probability and consequence of all ESLs. The San Juan and Norfolk EAE for the historical (1991–2009) and future scenarios is denoted as filled colored circles on the x-axis in Figs. 2C,F. For both cities, the historical EAE is small, < 1,000 (assumes protection from the 10-yr ESL), but differences emerge under RSLC. By 2070, the EAE for Norfolk increases to ∼16,000 (+2 °C) and 45,000 (+5 °C), while the EAE for San Juan remains < 1,000 for both scenarios. However, flood protection assumptions can greatly change the EAE and the EAE AF. For instance, assuming that Norfolk has no flood protection, the EAE AF for 2070 is 3.4, but if assuming protection from the 10-yr event, it increase to 13.7 (Table S-5). The current and future EAE at cities around the globe under different protection assumptions are tabulated in the supporting data files.

3.2 Extreme sea level allowances versus population exposure allowances

The map in Fig. 4 shows the expected population exposure allowance needed to maintain the historical EAE for each city under projected 2070 RSLC (+2 °C). The population exposure allowance assumes all cities are currently protected against the 10-yr ESL (i.e., $A_{min} = z_{10}$, where z_{10} is the local return level of the 10-yr event) and that the historical EAE is maintained by elevating all populations within each city by the same amount A (Sec. 2.4). Globally, the exposure allowance ranges from < 0 m (i.e., where expected RSLC is negative) to > 2 m. For some regions, the 100-yr ESL allowance is quite similar to the population exposure allowance (Western North America, Europe, and Eastern South America), but for others, the relationship between the two is less strong (e.g., Eastern North America). The 100-yr ESL allowance sometimes both over- and under-predicts the allowance needed to maintain the current EAE. For most cities, the population exposure allowance for 2070 is larger than the expected RSLC (Tables 3 and 4; Fig. S-3).

3.3 The choice of the metric may impact estimates of flood risk

Many consequences can result from the same hazard, and most risk metrics only consider one consequence. For example, using a population exposure metric in New York City would not account for two major airports that are currently exposed to the 100-yr ESL event (LaGuardia and John F. Kennedy International; Fig. S-6B). Furthermore, risks estimated using population exposure may vary when considering specific population subgroups. For example, low household income residents of New York City ($<$\$50,000 yr^{-1}) are projected to have expected exposure increases ∼4-6% greater than when considering all household incomes (2100; Table S-1; Fig. S-5). While these differences are small, those that emerge when considering property damage are much larger. In New York City, the current expected damage from a 100-yr ESL event is roughly \$4 billion. By 2100, this number is expected to grow by roughly 3 and 4 fold under a +2 °C and +5 °C GSAT stabilization scenario, respectively (assumes constant 2017 US\$; Table S-2).

4 Discussion and Conclusion

Physical ESL metrics do not consider the harms of a particular ESL event to human systems, natural resources, and to ecosystem services. By not distinguishing between hazard, exposure, and vulnerability, climate and sea-level scientists could misrepresent projected changes in coastal flood risk. Despite this, physical ESL metrics continue to be used in assessment reports and the scientific literature as proxies for estimating coastal flood risk under different climate change scenarios (Vitousek et al, 2017; Taherkhani et al, 2020; Buchanan et al, 2017; Kriebel et al, 2015; Frederikse et al, 2020; Garner et al, 2017; Oppenheimer et al, in press; Wong et al, 2014; Church et al, 2013; Sweet et al, 2017; Kopp et al, 2019a; Howard and Palmer, 2020). This misuse of terminology could lead to inaccuracies in risk communication and poor planning. Our analysis specifically calls out ESL AFs (frequency and return level) and ESL hazard allowances. First, ESL return level AFs may both over- and under-estimate flood exposure as shown by the city-level examples of San Juan and Norfolk, as well as within and across regions (Sec. 3.1). Both the current population exposure and the gradient of the population profile play a crucial role in determining the amplification of population exposure. Second, we show that sub-optimal flood protection design could occur if ESL allowances do not consider a specific consequence (e.g., population exposure; Sec. 3.2). However, within some regions, the population exposure allowance does not appreciably differ from the ESL hazard allowance (Fig. 4). Third, we illustrate how coastal flood exposure and risk assessments can be strongly dependent on the chosen exposure and risk metric by considering household income, the siting of critical infrastructure, and property damage (Sec. 3.3).

All risk metrics have limitations in what they are able to communicate. Choosing what consequences to include in an exposure or risk assessment is subjective and depends on the preferences and goals of flood managers. There is no "best" metric. Many measures of risk are possible and all tell a part of the same "risk story". However, metric choice is critical for determining what kinds of information can come from an exposure or risk assessment, including that which can inform decision-making (Kunreuther and Slovic, 1996; Slovic et al, 1982; Slovic, 1987). Such limitations point to the importance of choosing a broad and balanced set of metrics. While hazard metrics are essentially value-free, different stakeholders may have different opinions about what exposure or risk metric is most relevant. These factors may include practicality (i.e., ease of calculation) and suitability (i.e., informing specific risk management decisions) (NRC, 1996). In this paper we use current population exposure as an example of a viable metric for estimating societal exposure to coastal floods, but have noted that others are possible.

We acknowledge a number of caveats. First—and most importantly—we emphasize that this study does not make literal estimates of future population exposure to ESLs. Results presented in this paper are intended to highlight the implications of the ongoing misuse of hazard-based metrics to communicate coastal flood exposure and risk. The performance of our inundation modeling approach has not been extensively validated and is challenged by a lack of observed flood extents. Second, almost all coastal cities have developed over time with some margin of safety against ESLs, but including these defenses and any spatial variation within cities is challenging without obtaining detailed and accurate data. In the absence of this information, we make multiple assumptions regarding uniform protection for each city. The protection assumptions do not impact AFs above the height of the protection level, but can significantly impact integrated metrics that consider all ESLs and impacts, such as the EAE (Table S-5). We encourage future efforts to compile accurate information on urban flood protection levels around the world. Third, exposure analyses are most sensitive

to spatially-autocorrelated vertical errors in the DEM at local scales and when assessing population vulnerability at low elevations (e.g., < 0.5 m; Kulp and Strauss, 2019). The higher the elevation that population exposure is being assessed at (e.g., longer return periods, such as the 100-yr event), the less of an impact these errors will have on exposure (Kulp and Strauss, 2019). To assess the impact of elevation errors on population exposure AFs, we use the example of the 100-year ESL event in New York City (Fig. S-6A). Considering lidar topography as ground truth, we find that the EAE AFs are generally insensitive to errors in CoastalDEM; small differences only appear by 2100 for the +5 °C scenario (2.3 vs 2.6; Table S-4). This is despite CoastalDEM underestimating population exposure relative to lidar (connected components analysis not performed for this test; Tables S-3,S-4). We note that CoastalDEM was trained on lidar elevation data in the U.S., so locations outside the U.S. may be more sensitive.

In conclusion, we suggest that policy makers and climate risk communication efforts should avoid using physical ESL metrics as proxies for coastal flood risk. This includes avoiding language that conflates physical metrics with societal impacts (e.g., calling all ESLs "floods"). Not doing so may miss important societal aspects that are overlooked when only viewing through a physical science lens. Additionally, to better illustrate sea-level rise and coastal flood impacts, broadly speaking, multiple risk or exposure metrics should be presented when possible.

Acknowledgements We thank William V. Sweet (NOAA) for stimulating conversations about the limitations of applying extreme sea level frequency amplification factors. D. J. R. was supported by the Science, Technology, and Environmental Policy (STEP) Program at Princeton University. R. E. K. was supported by grants from the National Science Foundation (ICER-1663807, DGE-1633557), the National Aeronautics and Space Administration (80NSSC17K0698), and from the Rhodium Group (for whom he has previously worked as a consultant) as part of the Climate Impact Lab consortium. S. K. and B. H. S. were supported by National Science Foundation (ICER-1663807), the National Aeronautics and Space Administration (80NSSC17K0698), and the V. Kann Rasmussen Foundation. The 3-arcsecond (90-m) version of CoastalDEM used in this analysis is available at no cost from Climate Central for non-commercial research use. Code for generating sea-level projections is available in the following repositories on Github: ProjectSL (https://github.com/bobkopp/ProjectSL) and LocalizeSL (https://github.com/bobkopp/LocalizeSL). Code for generating extreme sea level projections is available in the following repositories on Github: hawaiiSL_process (https://github.com/dmr2/hawaiiSL_process), GPDfit (https://github.com/dmr2/GPDfit), and return_curves (https://github.com/dmr2/return_curves). The statements, findings, conclusions, and recommendations are those of the authors and do not necessarily reflect the views of the funding agencies.

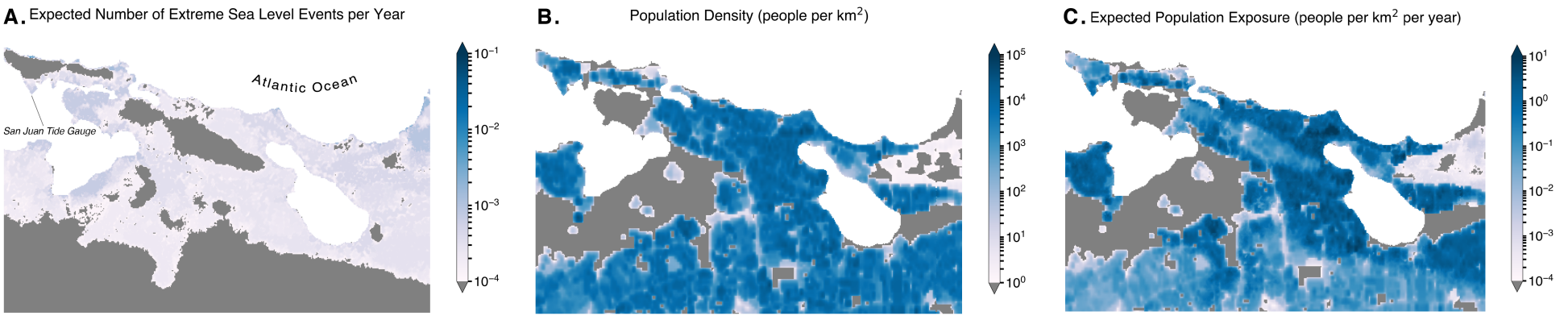

Fig. 1: **A.** A map of San Juan (Puerto Rico) showing the expected number of extreme sea level (ESL) events per year as estimated using 1) ESL return levels from the San Juan tide gauge (indicated), 2) ground elevation from CoastalDEM, and 3) the "bathtub" flood inundation method (Sec. S-1.3). **B.** Map showing population density (people per km^2) from the 2010 WorldPop global gridded population database (Tatem, 2017). **C.** Map showing the annual expected population exposure (people per km^2 per year)

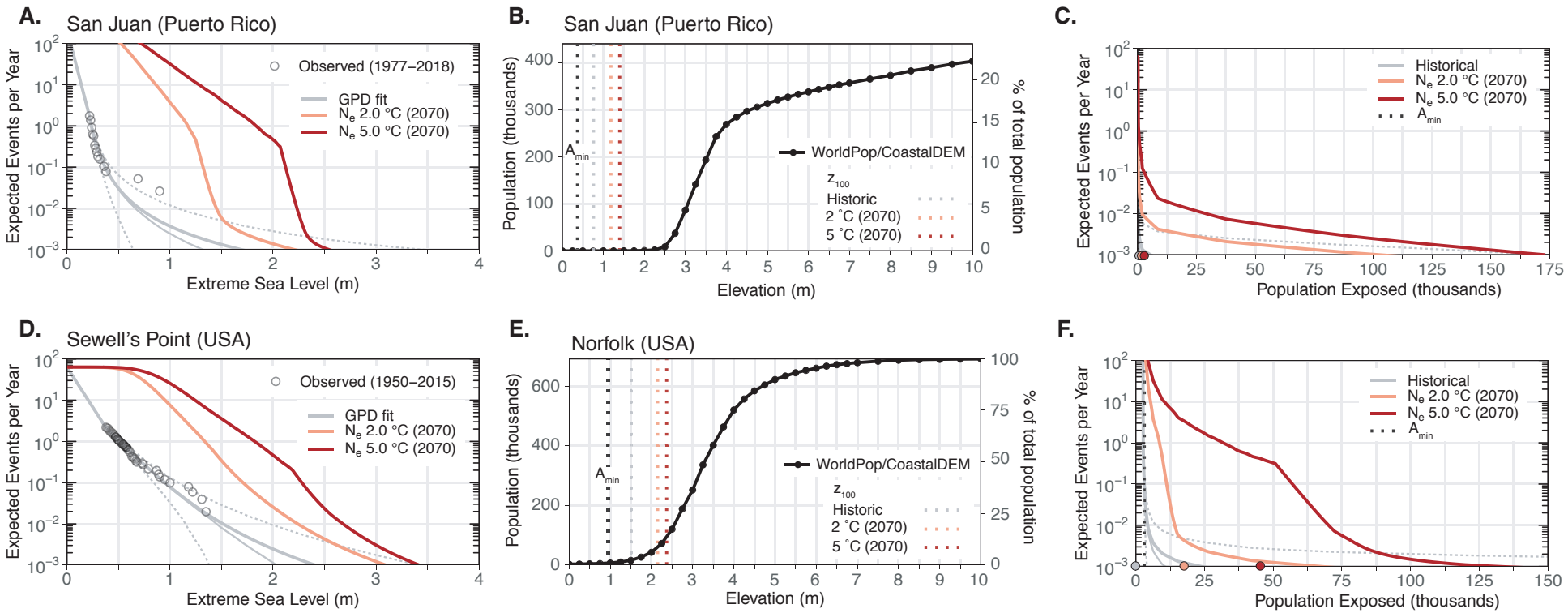

Fig. 2: **A.** Expected number of extreme sea level (ESL) events per year as a function of ESL height (meters above local mean higher high water; MHHW) calculated by fitting a generalized Pareto distribution (GPD) to tide gauge observations (open grey circles) at San Juan (Puerto Rico) for 1991–2009 mean sea level (MSL; thick grey line), projected relative sea-level rise (RSLR) in 2070 under a scenario in which global mean surface air temperature (GSAT) is stabilized in 2100 at +2 °C (orange line) and +5 °C (red line; GSAT relative to 1850–1900). Thin grey lines are the historical ESL return curves for the 5/50/95 percentiles of the GPD parameter uncertainty range (dotted/solid/dotted lines, respectively). **B.** A population exposure function that estimates the total population (left y-axis) and percent of total population (right y-axis) currently as risk of inundation as a function of ESL height (meters above MHHW) for San Juan (total population: 1.82 million). Filled black circles are population data from the 2010 WorldPop global gridded population database (Tatem, 2017) applied to the elevation surfaces of CoastalDEM (Kulp and Strauss, 2018). Linear interpolation is used to produce a continuous curve between the WorldPop data (black line). City boundaries are those as defined by Kelso and Patterson (2012) and may differ from actual political boundaries. Populations are assumed to remain constant in time. Denoted is the current level of protection (A_{min}), assumed to be the 10-yr ESL event, the height of the historical 100-yr ESL event (grey), and the expected heights of the 100-yr ESL event under a +2 °C (orange) and +5 °C (red) climate scenario. **C.** As for top left, but for the population exposed per event under 1991–2009 MSL (grey lines) and RSLR in 2070 under +2 °C (orange line) and +5 °C 2100 GSAT stabilization scenarios (red line). The projected future inundated population estimates assume that San Juan's population remains constant in time. Denoted are the assumptions of arbitrarily assuming that populations are protected below the height of the 10-yr ESL event. The expected annual population exposure (assuming protection from a 10-yr ESL event) is denoted with a filled colored circle on the x-axis for the historical period (grey) and for the +2 °C (orange) and +5 °C (red) scenarios. **Second Row:** As for Top Row, but for Norfolk (USA; total population: 695,000) using the expected number of ESL events from a tide gauge located at Sewell's Point (USA).

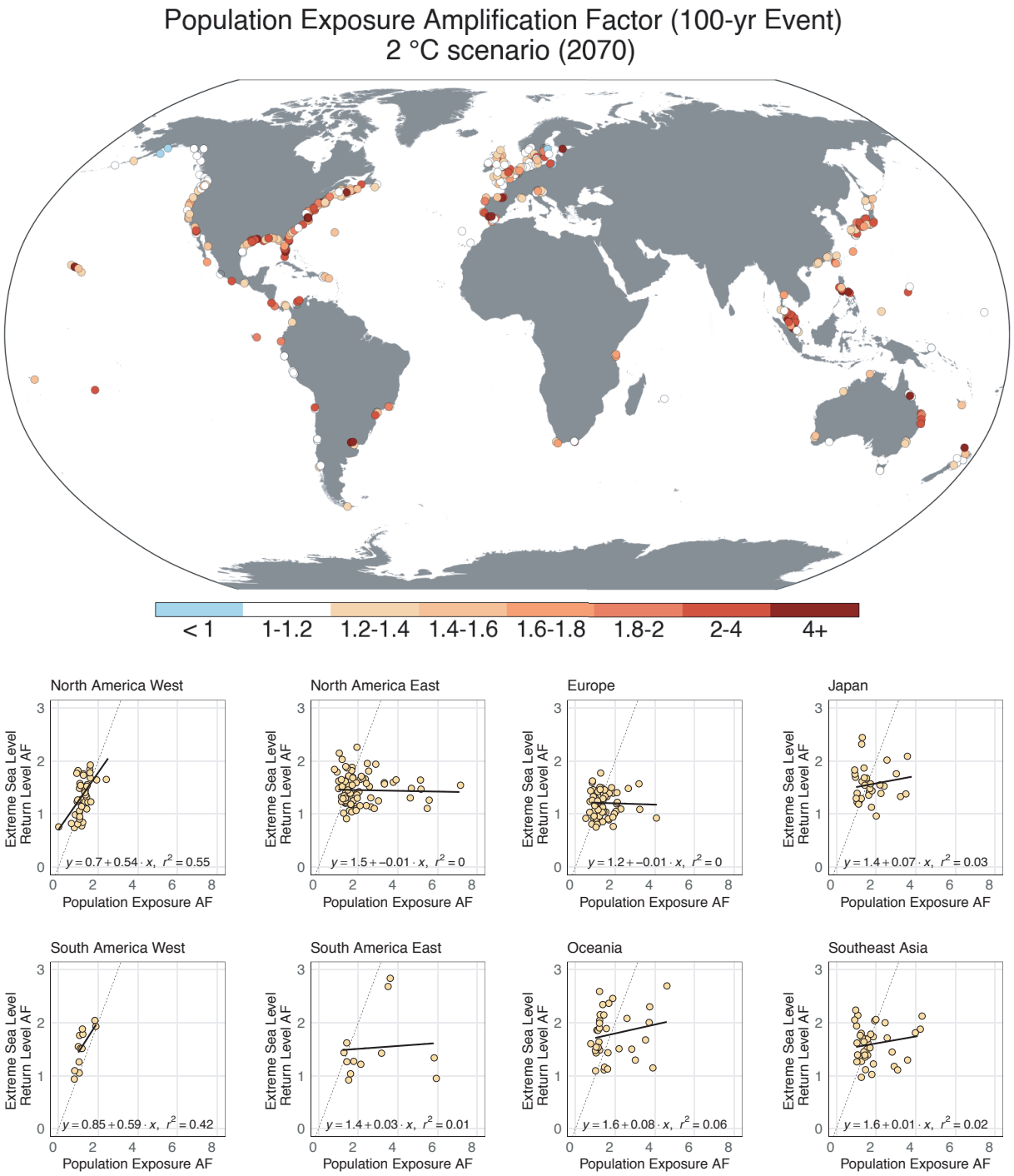

Fig. 3: **Map:** Population exposure AFs for cities for 2070 under a climate scenario where the global mean surface air temperature is stabilized in 2100 at +2 °C (relative to 1850–1900). Populations are assumed to remain constant in time. **Regional scatter plots:** Extreme sea level (ESL) return level AFs plotted against population exposure AFs for the 100-yr ESL event for 2070 for the same climate scenario as the map. A list of the cities in each defined region is given in the supporting data files. Note that some cities may not appear in the scatter plots if 1) current and future population inundation is zero, 2) the current inundation is zero but future inundation is non-zero (i.e., a population exposure AF of infinity), or 3) the population exposure AF is more than two times the standard deviation of all other cities within each region. Cities are not shown in the scatter plots if the population exposure AF is greater than two standard deviations from the mean of each region.

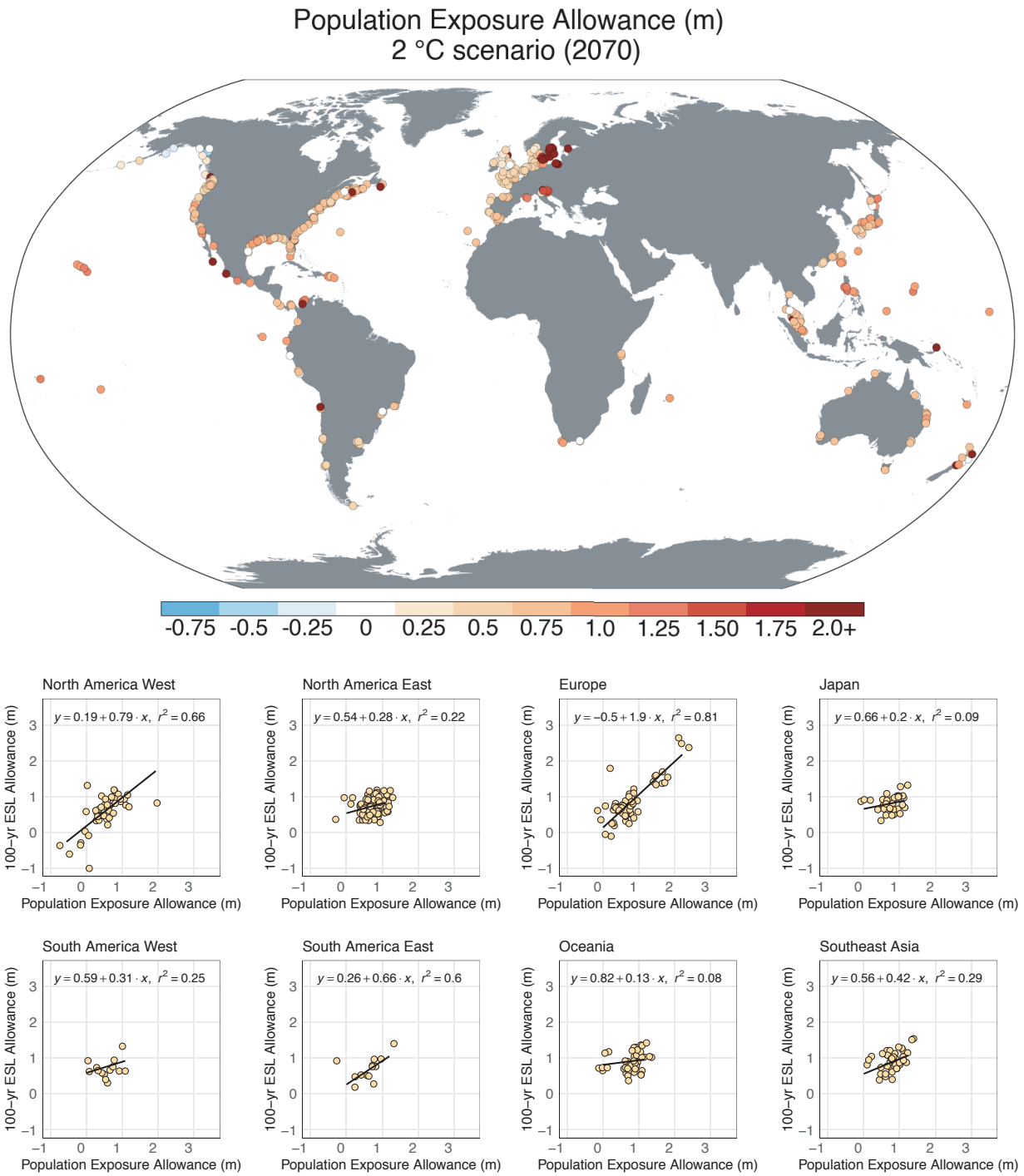

Fig. 4: **Map:** Population exposure allowances (also the design height of a flood protection strategy) for cities for 2070 under a climate scenario where the global mean surface air temperature is stabilized in 2100 at +2 °C (relative to 1850–1900). The population exposure allowance (also the design height of a flood protection strategy) maintains the historical annual expected population inundation exposure from extreme sea levels (ESLs) and assumes population distributions remain constant in time and that cities are protected from the current 10-yr extreme sea-level (ESL) event (1991–2009). Careful consideration should be given for cities in the Baltic and North Sea region. Difference of sign in modeled changes in ocean dynamics can lead to anomalously large allowances in comparison to relative sea level change (Fig. S-3). **Regional scatter plots:** ESL allowances for the 100-yr ESL event plotted against population exposure allowances for 2070 for the same climate scenario as the map. A list of the cities in each defined region is given in the supporting data files. Cities are not shown in the scatter plots if the population exposure allowance is greater than two standard deviations from the mean of each region.

100-yr ESL event			2070 (2.0 °C)					
	Historical		Physical metrics			Societal metrics		
City (Total population in thousands)	100-yr ESL (m)	% Pop exposed	RSLC (m)	ESL frequency AF	ESL level AF	Pop exposure AF	Pop exposed (thousands)	% increase
Buenos Aires, Argentina (11,980)	2.6 (2.1-3.3)	7.5%	0.4 (0.2-0.7)	3 (2-7)	1.2 (1.1-1.3)	1.5 (1.2-1.7)	1,321 (1,111-1,520)	3.5% (1.8-5.2%)
Copenhagen, Denmark (1,337)	1.1 (1.0-1.1)	1.5%	0.2 (-0.8-1.1)	991 (0-9677)	1.2 (0.3-2.1)	1.3 (0.0-3.2)	26 (0-63)	0.4% (-1.5-3.2%)
Dar es Salaam, Tanzania (2,322)	0.7 (0.6-0.7)	1.0%	0.5 (0.2-0.8)	2441 (254-6678)	1.7 (1.3-2.2)	1.7 (1.1-2.6)	39 (25-59)	0.7% (0.1-1.6%)
Hamburg, Germany (1,854)	4.0 (3.6-4.4)	14.9%	0.4 (0.1-0.7)	4 (2-9)	1.1 (1.0-1.2)	1.1 (1.0-1.2)	301 (285-320)	1.3% (0.4-2.3%)
Hong Kong, China (22,232)	1.8 (1.2-2.5)	32.9%	0.4 (0.1-0.8)	5 (1-12)	1.2 (1.1-1.4)	1.2 (1.1-1.4)	8,988 (7,788-10,111)	7.5% (2.1-12.6%)
Honolulu, HI, USA (466)	0.4 (0.3-0.4)	0.5%	0.5 (0.2-0.9)	12385 (942-14455)	2.4 (1.6-3.4)	4.6 (2.1-8.5)	11 (5-20)	1.8% (0.6-3.7%)
London, England (9,878)	0.9 (0.7-1.1)	1.8%	0.4 (0.2-0.7)	61 (4-188)	1.4 (1.2-1.7)	2.1 (1.4-2.9)	368 (252-515)	1.9% (0.8-3.4%)
Manila, Philippines (5,782)	0.8 (0.7-0.9)	36.5%	0.9 (0.6-1.2)	15443 (3322-*)	2.1 (1.8-2.5)	1.1 (1.1-1.2)	2,336 (2,249-2,440)	3.9% (2.4-5.7%)
New Orleans, LA, USA (711)	2.3 (1.2-4.1)	77.7%	1.0 (0.7-1.3)	4 (2-7)	1.4 (1.3-1.6)	1.2 (1.1-1.2)	643 (623-663)	12.7% (9.9-15.5%)
New York, NY, USA (12,520)	1.9 (1.5-2.3)	3.7%	0.6 (0.3-0.9)	11 (2-29)	1.3 (1.1-1.5)	1.4 (1.2-1.7)	654 (543-799)	1.5% (0.6-2.7%)
Norfolk, VA, USA (695)	1.5 (1.1-2.0)	2.3%	0.6 (0.4-1.0)	32 (4-81)	1.4 (1.3-1.6)	4.1 (2.2-7.3)	64 (35-114)	6.9% (2.8-14.2%)
Phuket, Thailand (159)	0.9 (0.8-1.0)	9.0%	0.5 (0.2-0.8)	1723 (37-7875)	1.5 (1.2-1.9)	1.2 (1.1-1.4)	17 (16-20)	1.9% (0.9-3.5%)
Rio de Janeiro, Brazil (9,110)	0.9 (0.8-1.1)	0.3%	0.5 (0.2-0.8)	992 (8-5242)	1.5 (1.2-1.9)	1.8 (1.3-2.5)	59 (43-80)	0.3% (0.1-0.5%)
San Diego, CA, USA (2,323)	0.7 (0.7-0.7)	0.2%	0.5 (0.2-0.8)	4726 (298-15431)	1.7 (1.4-2.2)	3.0 (1.6-5.7)	13 (7-25)	0.4% (0.1-0.9%)
San Juan, Puerto Rico (1,821)	0.7 (0.5-1.1)	0.0%	0.5 (0.2-0.8)	2918 (4-*)	1.7 (1.3-2.1)	1.4 (1.1-1.9)	0 (0-0)	0.0% (0.0-0.0%)
Shenzhen, China (12,518)	1.8 (1.2-2.6)	17.5%	0.4 (0.1-0.8)	5 (1-12)	1.2 (1.1-1.4)	1.2 (1.1-1.3)	2,651 (2,327-2,938)	3.6% (1.1-5.9%)
Sydney, Australia (3,483)	0.7 (0.7-0.7)	0.2%	0.4 (0.2-0.8)	3213 (60-16480)	1.6 (1.3-2.1)	1.2 (1.1-1.3)	9 (9-11)	0.0% (0.0-0.1%)
Tokyo, Japan (25,339)	1.5 (1.0-2.1)	5.5%	0.4 (0.1-0.7)	8 (1-18)	1.2 (1.1-1.5)	1.9 (1.1-3.0)	2,656 (1,610-4,278)	4.9% (0.8-11.3%)
Vancouver, Canada (1,810)	1.3 (1.1-1.6)	11.8%	0.2 (0.0-0.5)	28 (1-94)	1.2 (1.0-1.4)	1.0 (1.0-1.0)	218 (214-223)	0.2% (0.0-0.5%)

Table 1: Table listing both physical and societal extreme sea level (ESL) metrics for select major coastal cities. Given are the heights of the historical 100-yr ESL return period (meters relative to mean higher high water; expected/5th/95th percentile), the percent of the total population exposed to the expected 100-yr ESL event, 2070 probabilistic relative sea-level change (RSLC) (meters, relative to 1991–2009) from a climate scenario in which global mean surface air temperature (GSAT) is stabilized in 2100 at +2 °C (relative to 1850–1900; Bamber et al, 2019), ESL return period amplification factors (AFs) for the 100-yr ESL event, ESL return level AFs for the 100-yr ESL event, the population exposure AF, the estimated total population exposed to the future 100-yr ESL event (thousands), and the percent increase in the latter, relative the historical population exposure. The expected value and the 5/95 percentile of the estimate are given for each. The 5/95 percentile for the current ESL return period considers the uncertainty in the generalized Pareto distribution (GPD) parameters, while the 5/95 percentile for RSLC and AFs reflect the uncertainty from both contributions to local RSLC and from the GPD. The * denotes instances of when the height of the current 100-yr ESL event occurs more often than the present-day frequency of exceeding MHHW (given for each tide gauge in the supporting information). The mapping of tide gauges to cities is given in the supporting information.

100-yr ESL event			2070 (5.0 °C)					
	Historical		Physical metrics			Societal metrics		
City (Total population in thousands)	100-yr ESL (m)	% Pop exposed	RSLC (m)	ESL frequency AF	ESL level AF	Pop exposure AF	Pop exposed (thousands)	% increase
Buenos Aires, Argentina (11,980)	2.6 (2.1-3.3)	7.5%	0.6 (0.3-1.1)	8 (2-20)	1.2 (1.1-1.4)	1.6 (1.4-1.9)	1,449 (1,241-1,682)	4.6% (2.9-6.6%)
Copenhagen, Denmark (1,337)	1.1 (1.0-1.1)	1.5%	0.5 (0.1-1.0)	841 (10-5575)	1.5 (1.1-1.9)	1.6 (1.1-2.5)	31 (21-51)	0.9% (0.1-2.3%)
Dar es Salaam, Tanzania (2,322)	0.7 (0.6-0.7)	1.0%	0.7 (0.3-1.2)	4720 (620-6678)	2.1 (1.5-2.9)	2.3 (1.1-3.1)	52 (26-70)	1.3% (0.1-2.0%)
Hamburg, Germany (1,854)	4.0 (3.6-4.3)	14.9%	0.6 (0.3-1.1)	9 (2-22)	1.2 (1.1-1.3)	1.1 (1.1-1.2)	314 (293-338)	2.0% (0.9-3.3%)
Hong Kong, China (22,232)	1.8 (1.2-2.6)	32.9%	0.6 (0.2-1.2)	120 (2-155)	1.4 (1.1-1.7)	1.3 (1.2-1.5)	9,636 (8,437-10,847)	10.4% (5.0-15.9%)
Honolulu, HI, USA (466)	0.4 (0.3-0.4)	0.5%	0.8 (0.4-1.3)	14017 (14455-14455)	3.1 (2.0-4.7)	8.1 (3.2-18.4)	19 (7-43)	3.5% (1.1-8.6%)
London, England (9,878)	0.9 (0.7-1.1)	1.8%	0.6 (0.3-1.0)	223 (12-1242)	1.6 (1.3-2.1)	2.6 (1.8-4.1)	468 (310-728)	2.9% (1.3-5.6%)
Manila, Philippines (5,782)	0.8 (0.7-0.9)	36.5%	1.1 (0.7-1.6)	17547 (8662-*)	2.4 (1.9-3.0)	1.1 (1.1-1.2)	2,402 (2,276-2,597)	5.0% (2.8-8.4%)
New Orleans, LA, USA (711)	2.3 (1.2-4.2)	77.7%	1.2 (0.8-1.7)	94 (3-27)	1.5 (1.4-1.7)	1.2 (1.1-1.2)	655 (634-677)	14.4% (11.5-17.6%)
New York, NY, USA (12,520)	1.9 (1.5-2.3)	3.7%	0.8 (0.4-1.3)	228 (3-296)	1.4 (1.2-1.7)	1.6 (1.2-2.1)	738 (578-957)	2.2% (0.9-3.9%)
Norfolk, VA, USA (695)	1.5 (1.1-1.9)	2.3%	0.9 (0.5-1.4)	343 (7-1660)	1.6 (1.3-1.9)	6.6 (2.7-13.9)	104 (42-219)	12.6% (3.9-29.2%)
Phuket, Thailand (159)	0.9 (0.8-1.0)	9.0%	0.7 (0.3-1.2)	6012 (208-*)	1.7 (1.3-2.3)	1.4 (1.1-1.8)	19 (16-26)	3.2% (1.3-7.1%)
Rio de Janeiro, Brazil (9,110)	0.9 (0.8-1.1)	0.3%	0.7 (0.3-1.2)	3951 (30-14619)	1.7 (1.4-2.3)	2.2 (1.5-3.5)	71 (49-110)	0.4% (0.2-0.9%)
San Diego, CA, USA (2,323)	0.7 (0.7-0.7)	0.2%	0.7 (0.3-1.2)	9611 (798-15431)	2.0 (1.5-2.8)	4.5 (2.0-8.6)	20 (9-38)	0.7% (0.2-1.4%)
San Juan, Puerto Rico (1,821)	0.7 (0.5-1.1)	0.0%	0.7 (0.3-1.2)	10225 (10-*)	2.0 (1.5-2.7)	3.3 (1.2-5.4)	0 (0-1)	0.0% (0.0-0.0%)
Shenzhen, China (12,518)	1.8 (1.2-2.7)	17.4%	0.6 (0.2-1.2)	120 (2-155)	1.4 (1.1-1.7)	1.3 (1.1-1.4)	2,813 (2,496-3,131)	5.0% (2.5-7.6%)
Sydney, Australia (3,483)	0.7 (0.7-0.7)	0.2%	0.7 (0.3-1.1)	8942 (374-16480)	2.0 (1.5-2.7)	1.4 (1.1-2.6)	11 (9-21)	0.1% (0.0-0.4%)
Tokyo, Japan (25,339)	1.5 (1.0-2.2)	5.5%	0.6 (0.2-1.2)	455 (2-914)	1.4 (1.1-1.8)	2.6 (1.4-4.3)	3,635 (1,880-5,935)	8.9% (1.9-17.9%)
Vancouver, Canada (1,810)	1.3 (1.1-1.6)	11.8%	0.4 (0.1-0.9)	436 (2-1065)	1.3 (1.0-1.6)	1.0 (1.0-1.1)	221 (215-229)	0.4% (0.1-0.8%)

Table 2: As for Table 1, but for a climate scenario in which global mean surface air temperature (GSAT) is stabilized in 2100 at +5 °C (relative to 1850–1900; Bamber et al, 2019).

Allowances				2070 (2.0 °C)				
	Historical			Physical metrics		Societal metrics		
City (Total population in thousands)	100-yr ESL (m)	% Pop exposed	EAE (thousands)	RSLC (m)	100-yr ESL allowance	EAE (thousands)	% increase	Pop exposure allowance
Buenos Aires, Argentina (11,980)	2.6 (2.1-3.3)	7.5%	23	0.4 (0.2-0.7)	0.5	85	269.4%	0.5
Copenhagen, Denmark (1,337)	1.1 (1.0-1.1)	1.5%	2	0.2 (-0.8-1.1)	2.4	89	5481.4%	2.2
Dar es Salaam, Tanzania (2,322)	0.7 (0.6-0.7)	1.0%	1	0.5 (0.2-0.8)	1.0	46	3058.5%	0.8
Hamburg, Germany (1,854)	4.0 (3.6-4.4)	14.9%	24	0.4 (0.1-0.7)	0.5	73	207.1%	0.5
Hong Kong, China (22,232)	1.8 (1.2-2.5)	32.9%	524	0.4 (0.1-0.8)	0.5	5,611	970.8%	0.6
Honolulu, HI, USA (466)	0.4 (0.3-0.4)	0.5%	0	0.5 (0.2-0.9)	1.2	22	14353.0%	1.1
London, England (9,878)	0.9 (0.7-1.1)	1.8%	11	0.4 (0.2-0.7)	0.6	174	1504.1%	0.5
Manila, Philippines (5,782)	0.8 (0.7-0.9)	36.5%	156	0.9 (0.6-1.2)	1.3	2,350	1408.9%	1.2
New Orleans, LA, USA (711)	2.3 (1.2-4.1)	77.7%	36	1.0 (0.7-1.3)	1.0	475	1231.2%	1.1
New York, NY, USA (12,520)	1.9 (1.5-2.3)	3.7%	34	0.6 (0.3-0.9)	0.6	391	1056.1%	0.7
Norfolk, VA, USA (695)	1.5 (1.1-2.0)	2.3%	1	0.6 (0.4-1.0)	0.7	16	1271.2%	0.7
Phuket, Thailand (159)	0.9 (0.8-1.0)	9.0%	1	0.5 (0.2-0.8)	0.9	17	1541.3%	0.8
Rio de Janeiro, Brazil (9,110)	0.9 (0.8-1.1)	0.3%	3	0.5 (0.2-0.8)	0.8	50	1803.1%	0.8
San Diego, CA, USA (2,323)	0.7 (0.7-0.7)	0.2%	0	0.5 (0.2-0.8)	1.0	18	5635.2%	0.9
San Juan, Puerto Rico (1,821)	0.7 (0.5-1.1)	0.0%	0	0.5 (0.2-0.8)	0.7	0	232.5%	0.8
Shenzhen, China (12,518)	1.8 (1.2-2.6)	17.5%	160	0.4 (0.1-0.8)	0.5	1,730	980.7%	0.6
Sydney, Australia (3,483)	0.7 (0.7-0.7)	0.2%	1	0.4 (0.2-0.8)	0.9	9	1395.9%	0.8
Tokyo, Japan (25,339)	1.5 (1.0-2.1)	5.5%	98	0.4 (0.1-0.7)	0.5	1,104	1025.8%	0.6
Vancouver, Canada (1,810)	1.3 (1.1-1.6)	11.8%	18	0.2 (0.0-0.5)	0.4	177	866.2%	0.4

Table 3: Table listing both physical and societal extreme sea level (ESL) metrics for select major coastal cities. Given are the heights of the current 100-yr ESL return period [meters relative to mean higher high water (MHHW); expected/5th/95th percentile], the percent of the total population exposed to the expected 100-yr ESL events, the expected annual population exposure (EAE; thousands of people), 2070 probabilistic relative sea-level change (RSLC) (meters, relative to 1991–2009) from a climate scenario in which global mean surface air temperature (GSAT) is stabilized in 2100 at +2 °C (relative to 1850–1900; Bamber et al, 2019), the ESL allowance that maintains the frequency of the historical 100-yr event (meters above MHHW), the projected EAE (thousands), the percent increase in the EAE, and the population exposure allowance (meters above MHHW).

Allowances				2070 (5.0 °C)				
	Historical			Physical metrics		Societal metrics		
City (Total population in thousands)	100-yr ESL (m)	% Pop exposed	EAE (thousands)	RSLC (m)	100-yr ESL allowance	EAE (thousands)	% increase	Pop exposure allowance
Buenos Aires, Argentina (11,980)	2.6 (2.1-3.3)	7.5%	23	0.6 (0.3-1.1)	0.7	213	830.6%	0.8
Copenhagen, Denmark (1,337)	1.1 (1.0-1.1)	1.5%	2	0.5 (0.1-1.0)	1.1	32	1896.1%	0.9
Dar es Salaam, Tanzania (2,322)	0.7 (0.6-0.7)	1.0%	1	0.7 (0.3-1.2)	1.7	68	4493.5%	1.5
Hamburg, Germany (1,854)	4.0 (3.6-4.3)	14.9%	24	0.6 (0.3-1.1)	0.7	119	397.9%	0.7
Hong Kong, China (22,232)	1.8 (1.2-2.6)	32.9%	525	0.6 (0.2-1.2)	0.9	7,855	1396.5%	1.1
Honolulu, HI, USA (466)	0.4 (0.3-0.4)	0.5%	0	0.8 (0.4-1.3)	2.0	71	46941.1%	2.0
London, England (9,878)	0.9 (0.7-1.1)	1.8%	11	0.6 (0.3-1.0)	1.0	324	2888.1%	1.0
Manila, Philippines (5,782)	0.8 (0.7-0.9)	36.5%	156	1.1 (0.7-1.6)	2.0	2,563	1545.9%	1.9
New Orleans, LA, USA (711)	2.3 (1.2-4.2)	77.7%	36	1.2 (0.8-1.7)	1.3	559	1470.4%	1.7
New York, NY, USA (12,520)	1.9 (1.5-2.3)	3.7%	34	0.8 (0.4-1.3)	1.0	547	1517.9%	1.2
Norfolk, VA, USA (695)	1.5 (1.1-1.9)	2.3%	1	0.9 (0.5-1.4)	1.2	45	3745.6%	1.3
Phuket, Thailand (159)	0.9 (0.8-1.0)	9.0%	1	0.7 (0.3-1.2)	1.6	24	2152.5%	1.5
Rio de Janeiro, Brazil (9,110)	0.9 (0.8-1.1)	0.3%	3	0.7 (0.3-1.2)	1.4	83	3053.1%	1.4
San Diego, CA, USA (2,323)	0.7 (0.7-0.7)	0.2%	0	0.7 (0.3-1.2)	1.8	38	12326.7%	1.6
San Juan, Puerto Rico (1,821)	0.7 (0.5-1.1)	0.0%	0	0.7 (0.3-1.2)	1.5	1	995.1%	1.5
Shenzhen, China (12,518)	1.8 (1.2-2.7)	17.4%	160	0.6 (0.2-1.2)	0.9	2,336	1363.1%	1.1
Sydney, Australia (3,483)	0.7 (0.7-0.7)	0.2%	1	0.7 (0.3-1.1)	1.5	20	2995.9%	1.4
Tokyo, Japan (25,339)	1.5 (1.0-2.2)	5.5%	98	0.6 (0.2-1.2)	1.0	2,846	2809.1%	1.2
Vancouver, Canada (1,810)	1.3 (1.1-1.6)	11.8%	18	0.4 (0.1-0.9)	1.0	221	1107.6%	0.9

Table 4: As for Table 3, but for a climate scenario in which global mean surface air temperature (GSAT) is stabilized in 2100 at +5 °C (relative to 1850–1900; Bamber et al, 2019).

References

Arns A, Dangendorf S, Jensen J, et al (2017) Sea-level rise induced amplification of coastal protection design heights. Scientific Reports 7(1):40,171, DOI 10.1038/srep40171

Arns A, Wahl T, Wolff C, et al (2020) Non-linear interaction modulates global extreme sea levels, coastal flood exposure, and impacts. Nature Communications 11(1):1918, DOI 10.1038/s41467-020-15752-5

Bamber JL, Oppenheimer M, Kopp RE, Aspinall WP, Cooke RM (2019) Ice sheet contributions to future sea-level rise from structured expert judgment. Proceedings of the National Academy of Sciences 116(23):11,195–11,200, DOI 10.1073/pnas.1817205116

Bates PD, Dawson RJ, Hall JW, et al (2005) Simplified two-dimensional numerical modelling of coastal flooding and example applications. Coastal Engineering 52(9):793–810, DOI 10.1016/j.coastaleng.2005.06.001, URL https://linkinghub.elsevier.com/retrieve/pii/S037838390500075X

Breilh JF, Chaumillon E, Bertin X, Gravelle M (2013) Assessment of static flood modeling techniques: application to contrasting marshes flooded during Xynthia (western France). Natural Hazards and Earth System Sciences 13(6):1595–1612, DOI 10.5194/nhess-13-1595-2013, URL https://nhess.copernicus.org/articles/13/1595/2013/

Buchanan MK, Kopp RE, Oppenheimer M, Tebaldi C (2016) Allowances for evolving coastal flood risk under uncertain local sea-level rise. Climatic Change DOI 10.1007/s10584-016-1664-7

Buchanan MK, Oppenheimer M, Kopp RE (2017) Amplification of flood frequencies with local sea level rise and emerging flood regimes. Environmental Research Letters 12(6), DOI 10.1088/1748-9326/aa6cb3

Caldwell PC, Merrifield MA, Thompson PR (2015) Sea level measured by tide gauges from global oceans — the Joint Archive for Sea Level holdings (NCEI Accession 0019568). NOAA National Centers for Environmental Information Dataset

Church JA, Clark PU, et al (2013) Chapter 13: Sea level change. In: Stocker TF, Qin D, Plattner GK, et al (eds) Climate Change 2013: the Physical Science Basis, Cambridge University Press

Coles S (2001a) Classical Extreme Value Theory and Models. In: An Introduction to Statistical Modeling of Extreme Values, Springer, chap 3

Coles S (2001b) Threshold Models. In: An Introduction to Statistical Modeling of Extreme Values, Springer, chap 4

Cunnane C (1973) A particular comparison of annual maxima and partial duration series methods of flood frequency prediction. Journal of Hydrology 18(3-4):257–271, DOI 10.1016/0022-1694(73)90051-6

Dahl KA, Fitzpatrick MF, Spanger-Siegfried E (2017) Sea level rise drives increased tidal flooding frequency at tide gauges along the U.S. East and Gulf Coasts: Projections for 2030 and 2045. PLOS ONE 12(2):e0170,949, DOI 10.1371/journal.pone.0170949, URL https://journals.plos.org/plosone/article?id=10.1371/journal.pone.0170949, publisher: Public Library of Science

Diaz DB (2016) Estimating global damages from sea level rise with the Coastal Impact and Adaptation Model (CIAM). Climatic Change 137(1-2):143–156, DOI 10.1007/s10584-016-1675-4

Familkhalili R, Talke SA (2016) The effect of channel deepening on tides and storm surge: A case study of Wilmington, NC. Geophysical Research Letters 43(17):9138–9147, DOI 10.1002/2016GL069494, URL https://agupubs.onlinelibrary.wiley.com/doi/abs/10.1002/2016GL069494, _eprint: https://agupubs.onlinelibrary.wiley.com/doi/pdf/10.1002/2016GL069494

Farr TG, Rosen PA, Caro E, et al (2007) The Shuttle Radar Topography Mission. Reviews of Geophysics 45(2), DOI 10.1029/2005RG000183

Frederikse T, Buchanan MK, Lambert E, et al (2020) Antarctic Ice Sheet and emission scenario controls on 21st-century extreme sea-level changes. Nature Communications 11(1):1–11, DOI 10.1038/s41467-019-14049-6

Gallien T (2016) Validated coastal flood modeling at Imperial Beach, California: Comparing total water level, empirical and numerical overtopping methodologies. Coastal Engineering 111:95–104, DOI 10.1016/j.coastaleng.2016.01.014, URL https://linkinghub.elsevier.com/retrieve/pii/S0378383916300059

Garner AJ, Mann ME, Emanuel KA, et al (2017) Impact of climate change on New York City's coastal flood hazard: Increasing flood heights from the preindustrial to 2300 CE. PNAS pp 1–6, DOI 10.1073/pnas.1703568114

Ghanbari M, Arabi M, Obeysekera J, Sweet W (2019) A Coherent Statistical Model for Coastal Flood Frequency Analysis Under Nonstationary Sea Level Conditions. Earth's Future DOI 10.1029/2018EF001089

Gregory JM, Griffies SM, Hughes CW, et al (2019) Concepts and Terminology for Sea Level: Mean, Variability and Change, Both Local and Global. Surveys in Geophysics 40(6):1251–1289, DOI 10.1007/s10712-019-09525-z

Hallegatte S, Green C, Nicholls RJ, Corfee-Morlot J (2013) Future flood losses in major coastal cities. Nature Climate Change 3(9):802–806, DOI 10.1038/nclimate1979

Hanson S, Nicholls R, Ranger N, et al (2011) A global ranking of port cities with high exposure to climate extremes. Climatic Change 104(1):89–111, DOI 10.1007/s10584-010-9977-4

Hauer M, Hardy R, Kulp S, et al (2020) A framework for classifying and assessing sea level rise risk. SocArXiv DOI 10.31235/osf.io/tf6rj

Hauer ME (2017) Migration induced by sea-level rise could reshape the us population landscape. Nature Clim Change 7(5):321–325, URL http://dx.doi.org/10.1038/nclimate3271

Hauer ME, Evans JM, Mishra DR (2016) Millions projected to be at risk from sea-level rise in the continental United States. Nat Clim Chang (March), DOI 10.1038/nclimate2961, URL http://www.nature.com/doifinder/10.1038/nclimate2961

Hausfather Z, Peters GP (2020) Emissions – the 'business as usual' story is misleading. Nature 577(7792):618–620, DOI 10.1038/d41586-020-00177-3

Hinkel J, Lincke D, Vafeidis AT, et al (2014) Coastal flood damage and adaptation costs under 21st century sea-level rise. Proceedings of the National Academy of Sciences of the United States of America 111(9):3292–7, DOI 10.1073/pnas.1222469111

Howard T, Palmer MD (2020) Sea-level rise allowances for the UK. Environmental Research Communications 2(3):035,003, DOI 10.1088/2515-7620/ab7cb4, URL https://doi.org/10.1088%2F2515-7620%2Fab7cb4, publisher: IOP Publishing

Hunter J (2012) A simple technique for estimating an allowance for uncertain sea-level rise. Climatic Change 113:239–252, DOI 10.1007/s10584-011-0332-1

Hunter J, Church J, White N, Zhang X (2013) Towards a global regionally varying allowance for sea-level rise. Ocean Engineering 71:17 – 27, DOI 10.1016/j.oceaneng.2012.12.041

Hunter JR, Woodworth PL, Wahl T, Nicholls RJ (2017) Using global tide gauge data to validate and improve the representation of extreme sea levels in flood impact studies. Global and Planetary Change 156:34–45, DOI 10.1016/j.gloplacha.2017.06.007

Jevrejeva S, Jackson LP, Grinsted A, Lincke D, Marzeion B (2018) Flood damage costs under the sea level rise with warming of 1.5 °C and 2.0 °C. Environ Res Lett 13(074014):11, DOI 10.1088/1748-9326/aacc76

Jongman B, Ward PJ, Aerts JCJH (2012) Global exposure to river and coastal flooding: Long term trends and changes. Global Environmental Change 22(4):823–835, DOI 10.1016/j.gloenvcha.2012.07.004, URL http://www.sciencedirect.com/science/article/pii/S0959378012000830

Kelso NV, Patterson T (2012) World Urban Areas, LandScan, 1:10 million

Kirezci E, Young IR, Ranasinghe R, et al (2020) Projections of global-scale extreme sea levels and resulting episodic coastal flooding over the 21st Century. Scientific Reports 10(1):11,629, DOI 10.1038/s41598-020-67736-6, URL https://www.nature.com/articles/s41598-020-67736-6, number: 1 Publisher: Nature Publishing Group

Knapp KR, Kruk MC, Levinson DH, Diamond HJ, Neumann CJ (2010) The International Best Track Archive for Climate Stewardship (IBTrACS). Bulletin of the American Meteorological Society 91(3):363–376, DOI 10.1175/2009BAMS2755.1

Kopp RE, Horton RM, Little CM, et al (2014) Probabilistic 21st and 22nd century sea-level projections at a global network of tide gauge sites. Earth's Future 2:383–406, DOI 10.1002/2014EF000239

Kopp RE, Andrews CJ, Garner A, et al (2019a) New Jersey's Rising Seas and Changing Coastal Storms: Report of the 2019 Science and Technical Advisory Panel. Prepared for the New Jersey Department of Environmental Protection, Rutgers, The State University of New Jersey, New Brunswick, NJ

Kopp RE, Gilmore EA, Little CM, et al (2019b) Usable Science for Managing the Risks of Sea-Level Rise. Earth's Future 7(12):1235–1269, DOI 10.1029/2018EF001145

Kriebel DL, Geiman JD, Henderson GR (2015) Future Flood Frequency under Sea-Level Rise Scenarios. Journal of Coastal Research 315:1078–1083, DOI 10.2112/JCOASTRES-D-13-00190.1

Kulp S, Strauss BH (2017) Rapid escalation of coastal flood exposure in US municipalities from sea level rise. Climatic Change 142(3-4):477–489, DOI 10.1007/s10584-017-1963-7

Kulp SA, Strauss BH (2018) CoastalDEM: A global coastal digital elevation model improved from SRTM using a neural network. Remote Sensing of Environment 206:231–239, DOI 10.1016/j.rse.2017.12.026

Kulp SA, Strauss BH (2019) New elevation data triple estimates of global vulnerability to sea-level rise and coastal flooding. Nature Communications 10(1):4844, DOI 10.1038/s41467-019-12808-z

Kunreuther H, Slovic P (1996) Science, Values, and Risk. The Annals of the American Academy of Political and Social Science 545(1):116–125, DOI 10.1177/0002716296545001012

Lang M, Ouarda TBMJ, Bobée B (1999) Towards operational guidelines for over-threshold modeling. Journal of Hydrology 225(3):103–117, DOI 10.1016/S0022-1694(99)00167-5

Lichter M, Vafeidis AT, Nicholls RJ (2011) Exploring Data-Related Uncertainties in Analyses of Land Area and Population in the "Low-Elevation Coastal Zone" (LECZ). Journal of Coastal Research 27(4):757–768, DOI 10.2112/JCOASTRES-D-10-00072.1, URL https://bioone.org/journals/journal-of-coastal-research/volume-27/issue-4/JCOASTRES-D-10-00072.1/Exploring-Data-Related-Uncertainties-in-Analyses-of-Land-Area-and/10.2112/JCOASTRES-D-10-00072.1.full

McGranahan G, Balk D, Anderson B (2007) The rising tide: assessing the risks of climate change and human settlements in low elevation coastal zones. Environment and Urbanization 19(1):17–37, DOI 10.1177/0956247807076960, URL https://doi.org/10.1177/0956247807076960, publisher: SAGE Publications Ltd

Melet A, Meyssignac B, Almar R, Le Cozannet G (2018) Under-estimated wave contribution to coastal sea-level rise. Nature Climate Change 8(3):234–239, DOI 10.1038/s41558-018-0088-y

Menéndez M, Woodworth PL (2010) Changes in extreme high water levels based on a quasi-global tide-gauge data set. Journal of Geophysical Research: Oceans 115(10):1–15, DOI 10.1029/2009JC005997, iSBN: 2156-2202

Merkens JL, Reimann L, Hinkel J, Vafeidis AT (2016) Gridded population projections for the coastal zone under the Shared Socioeconomic Pathways. Global and Planetary Change 145:57–66, DOI 10.1016/j.gloplacha.2016.08.009, URL http://dx.doi.org/10.1016/j.gloplacha.2016.08.009

Moore FC, Obradovich N (2020) Using remarkability to define coastal flooding thresholds. Nature Communications 11(1):530, DOI 10.1038/s41467-019-13935-3, URL https://www.nature.com/articles/s41467-019-13935-3, number: 1 Publisher: Nature Publishing Group

Muis S, Verlaan M, Winsemius HC, Aerts JC, Ward PJ (2016) A global reanalysis of storm surge and extreme sea levels (1979-2014). Nature Communications 7(May):1–11, DOI 10.1038/ncomms11969

Muis S, Verlaan M, Nicholls RJ, et al (2017) A comparison of two global datasets of extreme sea levels and resulting flood exposure. Earth's Future 5(4):379–392, DOI 10.1002/2016EF000430

Neumann B, Vafeidis AT, Zimmermann J, Nicholls RJ (2015) Future coastal population growth and exposure to sea-level rise and coastal flooding - A global assessment. PLoS One 10(3), DOI 10.1371/journal.pone.0118571

Nicholls RJ, Hanson S, Herweijer C, et al (2008) Ranking Port Cities with High Exposure and Vulnerability to Climate Extremes: Exposure Estimates. OECD Environment Working Papers No. 1, Organisation for Economic Co-operation and Development (OECD), Paris, France

NOAA (2020) NOAA Digital Coast Coastal Lidar. URL https://coast.noaa.gov/digitalcoast/

NRC (1996) Understanding Risk. Informing Decisions in a Democratic Society. National Academy Press, National Research Council, Washington, D.C.

NYC Planning (2018) MapPLUTO database. data retrived from the NYC Planning Department: https://www1.nyc.gov/site/planning/data-maps/open-data/dwn-pluto-mappluto.page

Oppenheimer M, Glavovic B, Hinkel J, et al (in press) Chapter 4: Sea level rise and implications for low lying islands, coasts and communities. In: Pörtner HO, Roberts D, Masson-Delmotte V, et al (eds) IPCC Special Report on the Ocean and Cryosphere in a Changing Climate, Intergovernmental Panel on Climate Change (IPCC)

Parker B, Hess K, Milbert D, Gill S (2003) A national vertical datum transformation tool. Sea Technology 44(9):10–15

Pugh D, Woodworth P (2014) Sea-Level Science: Understanding Tides, Surges, Tsunamis and Mean Sea-Level Changes, 2nd edn. Cambridge University Press, Cambridge, UK

Ramirez JA, Lichter M, Coulthard TJ, Skinner C (2016) Hyper-resolution mapping of regional storm surge and tide flooding: comparison of static and dynamic models. Natural Hazards 82(1):571–590, DOI 10.1007/

s11069-016-2198-z, URL http://link.springer.com/10.1007/s11069-016-2198-z

Rasmussen DJ, Bittermann K, Buchanan MK, et al (2018) Extreme sea level implications of 1.5 °C, 2.0 °C, and 2.5 °C temperature stabilization targets in the 21st and 22nd centuries. Environmental Research Letters 13(3):034,040, DOI 10.1088/1748-9326/aaac87

Rasmussen DJ, Buchanan MK, Kopp RE, Oppenheimer M (2020) A Flood Damage Allowance Framework for Coastal Protection With Deep Uncertainty in Sea Level Rise. Earth's Future 8(3), DOI 10.1029/2019EF001340

Schindelegger M, Green JaM, Wilmes SB, Haigh ID (2018) Can We Model the Effect of Observed Sea Level Rise on Tides? Journal of Geophysical Research: Oceans 123(7):4593–4609, DOI 10.1029/2018JC013959, URL https://agupubs.onlinelibrary.wiley.com/doi/abs/10.1029/2018JC013959, _eprint: https://agupubs.onlinelibrary.wiley.com/doi/pdf/10.1029/2018JC013959

Scussolini P, Aerts JCJH, Jongman B, et al (2016) FLOPROS: an evolving global database of flood protection standards. Natural Hazards and Earth System Sciences 16(5):1049–1061, DOI 10.5194/nhess-16-1049-2016, URL https://nhess.copernicus.org/articles/16/1049/2016/

Seenath A, Wilson M, Miller K (2016) Hydrodynamic versus GIS modelling for coastal flood vulnerability assessment: Which is better for guiding coastal management? Ocean & Coastal Management 120:99–109, DOI 10.1016/j.ocecoaman.2015.11.019, URL https://linkinghub.elsevier.com/retrieve/pii/S0964569115300685

Slangen A, Hunter J, Woodworth P, et al (2017) The Impact of Uncertainties in Ice Sheet Dynamics on Sea-Level Allowances at Tide Gauge Locations. Journal of Marine Science and Engineering 5(2):21, DOI 10.3390/jmse5020021

Slovic P (1987) Perception of risk. Science 236(4799):280–285, DOI 10.1126/science.3563507

Slovic P, Fischhoff B, Lichtenstein S (1982) Facts versus fears: Understanding perceived risk. In: Kahneman D, Slovic P, Tversky A (eds) Judgment under Uncertainty, 1st edn, Cambridge University Press, pp 463–490, DOI 10.1017/CBO9780511809477.034

Sobel AH, Camargo SJ, Hall TM, et al (2016) Human influence on tropical cyclone intensity. Science 353(6296):242–246, DOI 10.1126/science.aaf6574, URL http://science.sciencemag.org/content/353/6296/242, http://science.sciencemag.org/content/353/6296/242.full.pdf

Sweet WV, Park J (2014) From the extreme to the mean: Acceleration and tipping points of coastal inundation from sea level rise. Earth's Future 2(12):579–600, DOI 10.1002/2014EF000272, 2014EF000272

Sweet WV, Kopp RE, Weaver CP, et al (2017) Global and regional sea level rise scenarios for the United States. Technical Report NOS CO-OPS 083, National Oceanic and Atmospheric Administration

Taherkhani M, Vitousek S, Barnard PL, et al (2020) Sea-level rise exponentially increases coastal flood frequency. Scientific Reports 10(1):1–17, DOI 10.1038/s41598-020-62188-4

Talke SA, Orton P, Jay DA (2014) Increasing storm tides in New York Harbor, 1844–2013. Geophysical Research Letters 41(9):3149–3155, DOI 10.1002/2014GL059574, URL https://agupubs.onlinelibrary.wiley.com/doi/abs/10.1002/2014GL059574, _eprint: https://agupubs.onlinelibrary.wiley.com/doi/pdf/10.1002/2014GL059574

Tatem AJ (2017) WorldPop, open data for spatial demography. Scientific Data 4(1):1–4, DOI 10.1038/sdata.2017.4

Tebaldi C, Strauss BH, Zervas CE (2012) Modelling sea level rise impacts on storm surges along US coasts. Environmental Research Letters 7:014,032, DOI 10.1088/1748-9326/7/1/014032

UNFCCC (2015) Report of the Conference of the Parties on its twenty-first session, held in Paris from 30 November to 13 December 2015, UNFCCC

Vitousek S, Barnard PL, Fletcher CH, et al (2017) Doubling of coastal flooding frequency within decades due to sea-level rise. Scientific Reports 7(1):1–9, DOI 10.1038/s41598-017-01362-7

Vousdoukas MI, Voukouvalas E, Mentaschi L, et al (2016) Developments in large-scale coastal flood hazard mapping. Natural Hazards and Earth System Sciences 16(8):1841–1853, DOI 10.5194/nhess-16-1841-2016, URL https://nhess.copernicus.org/articles/16/1841/2016/

Wahl T, Haigh ID, Nicholls RJ, et al (2017) Understanding extreme sea levels for broad-scale coastal impact and adaptation analysis. Nature Communications 8(May):16,075, DOI 10.1038/ncomms16075

Walsh KJE, McBride JL, Klotzbach PJ, et al (2016) Tropical cyclones and climate change. WIREs Climate Change 7(1):65–89, DOI 10.1002/wcc.371, URL http://onlinelibrary.wiley.com/doi/abs/10.1002/wcc.371, _eprint: https://onlinelibrary.wiley.com/doi/pdf/10.1002/wcc.371

Weyer NM (In press) Appendix I: Glossary. In: Cifuentes-Jara M, Frölicher T, Jackson M, Kudela RM, et al (eds) IPCC Special Report on the Ocean and Cryosphere in a Changing Climate, Intergovernmental Panel on Climate Change (IPCC)

Wong PP, Losada IJ, Gattuso JP, et al (2014) Coastal systems and low-lying areas. In: Field CB, Barros VR, Dokken DJ, et al (eds) Climate Change 2014: Impacts, Adaptation, and Vulnerability. Part A: Global and Sectoral Aspects. Contribution of Working Group II to the Fifth Assessment Report of the Intergovernmental Panel of Climate Change, Cambridge University Press, Cambridge, United Kingdom and New York, NY, USA, pp 361–409

Woodworth PL, Hunter JR, Marcos M, et al (2016) Towards a global higher-frequency sea level dataset. Geoscience Data Journal 3(2):50–59, DOI 10.1002/gdj3.42

Xian S, Yin J, Lin N, Oppenheimer M (2018) Influence of risk factors and past events on flood resilience in coastal megacities: Comparative analysis of NYC and Shanghai. Science of the Total Environment 610-611:1251–1261, DOI 10.1016/j.scitotenv.2017.07.229

Supplementary Information

S-1 Supplemental Methods

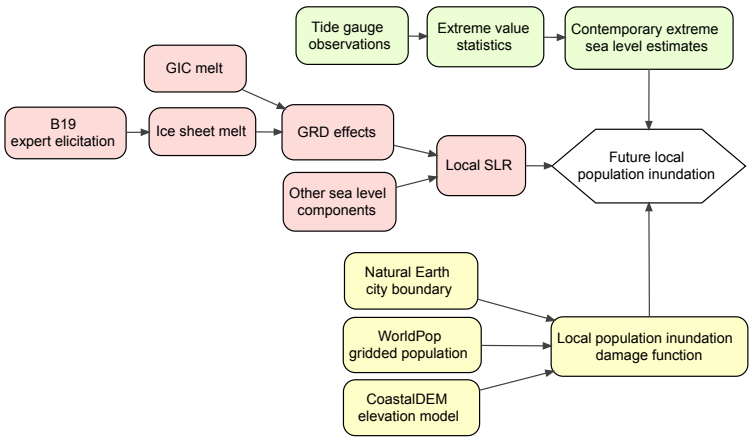

Fig. S-1: Flow of information used in this study to produce projected local population inundation estimates (white hexagon). Green rectangles are for extreme sea level estimation. Red rectangles are for sea-level rise projections. Yellow rectangles are for local population inundation estimates. B19 is Bamber et al (2019); SLR is sea-level rise; GIC are glaciers and ice caps; GRD are gravitational, rotational, and deformational effects; "Other sea level components" includes land water storage, oceanographic processes, and non-climatic background changes, such as glacial-isostatic adjustment.

S-1.1 Estimating extreme sea levels

We use long-term records of hourly or sub-hourly sea level observations from quality controlled tide gauges from the University of Hawaii Sea Level Center[4] and also supplement with other tide gauges from the GESLA2 data set (Woodworth et al, 2016). We limit our use of tide gauge records to only those that have record lengths $>$ 30 consecutive years in which each year has $>$ 80 percent of observations available. In total, we use 360 unique tide gauges, with median and average record lengths of 48 and $\sim$54 years, respectively (a list of the tide gauges used is given in the supporting information). For each day in the tide gauge record with $>$12 hours of data, we estimate the daily maximum sea level. We note that this temporal resolution only facilitates the estimation of still-water heights and is likely not sufficient to capture wave setup and swash contributions, which can be significant (Melet et al, 2018; Arns et al, 2017). To isolate the variation in extreme sea levels (ESLs), we remove the effect of mean sea level (MSL) change by subtracting the annual MSL from each daily maximum value (i.e., values are de-trended). The de-trended daily maximum tide values are then referenced to local mean higher high water (MHHW; relative to the de-trended mean sea level), defined as the average highest high tide at the tide gauge over a given period (here, either 1993–2012 or the last available 19-year period in the record). Daily maximum sea levels that are 1) above the 99th percentile and 2) within 3 days of

[4] retrieved from: https://uhslc.soest.hawaii.edu, January 2020; (Caldwell et al, 2015)

each other are de-clustered to meet the statistical independence assumption of the extreme value approach (below).

We estimate the present-day probability of ESLs by applying extreme value theory to long-term hourly tide gauge records. Extreme value theory is a statistical extrapolation method that fits an extreme value distribution to empirical data in order to estimate the likelihood of events too rare to appear in an observational record (e.g., determining the height of 100-yr ESL event from a 30-yr record of tide gauge data). Following previous studies (Tebaldi et al, 2012; Buchanan et al, 2017; Rasmussen et al, 2018; Frederikse et al, 2020; Wahl et al, 2017), we estimate the annual expected number of ESL events of various heights at each tide gauge using a generalized Pareto distribution (GPD; Coles, 2001b,a). The GPD is a peaks over threshold modeling approach that describes the probability of a given ESL height conditional on the exceedance of a threshold (assumed to be Poisson distributed with mean λ). Various extreme value distributions and approaches to implement them have been proposed (Coles, 2001a), but in the case of ESL estimation there currently is not an agreed upon "best approach". Depending on the specific project goals, a particular extreme value modeling strategy may be preferred over another. For example, if the tide gauge record is short, a peaks over threshold approach that uses sub-annual extremes may be preferred over an approach that only uses annual maximums (Lang et al, 1999; Cunnane, 1973). The GPD has the advantage over other generalized extreme value models in that 1) unlike the annual maximum flood value modeling approach, it can accommodate sub-annual observations (i.e., retain more information), 2) unlike the more restrictive Gumbel distribution (Buchanan et al, 2017), it includes a parameter that allows for the flexibility for the distribution to take on different shapes (shape parameter, ξ, and its value depends on the characteristics of the underlying data), and 3) it can be combined with a Poisson rate parameter (λ) to translate ESL exceedance probabilities into expected numbers of annual ESL exceedances. The latter may be more intuitive and thus better for communicating the frequency of ESL events. Increases or decreases in storminess could change λ, but is not considered in this study. For a given tide gauge, the annual expected number of exceedances of height z is given by $N(z)$:

$$N(z) = \begin{cases} \lambda \left(1 + \frac{\xi(z-\mu)}{\sigma}\right)^{-\frac{1}{\xi}} & \text{for } \xi \neq 0 \\ \lambda \exp(-\frac{z-\mu}{\sigma}) & \text{for } \xi = 0 \end{cases} \tag{S-1}$$

where the shape parameter (ξ) governs the curvature and upward statistical limit of $N(z)$, the scale parameter (σ) characterizes the variability in the exceedances, and the location parameter (μ) is the threshold water-level above which return levels are estimated with the GPD—here the 99th percentile of daily maximum sea levels. Observed GPD threshold exceedances and the fitted GPD $N(z)$ for tide gauges located at San Juan (Puerto Rico) and Sewell's Point (Norfolk, USA) are given in Figs. 2A,D. The GPD parameters for all tide gauges are given in the supporting data files.

Selecting the threshold μ is critical element of the peaks over threshold approach. If the threshold is too low, it could bias the estimates because the included values may not be extreme enough. On the other hand, if the threshold is too high, the variance might be too large because too few points are being included in the analysis (Lang et al, 1999). Here, the 99th percentile is used because it generally is above the highest seasonal tide, balances the bias-variance trade-off in the GPD parameter estimation (Tebaldi et al, 2012) and has been found to perform well at global scales (Wahl et al, 2017). The location parameter μ shifts as MSL changes. The storm climates and hydrodynamic characteristics of each site result in differences in the shape parameter (ξ) across sites. ESL frequency distributions with $\xi > 0$ are "heavy tailed", due to a larger variation in extremes (e.g., existence of tropical and extra-tropical cyclones). Distributions with $\xi < 0$ are "thin tailed" and have a statistical upper bound on ESLs. The GPD parameters are estimated using maximum likelihood, and their uncertainty is calculated from their estimated covariance matrix and is sampled using a Latin hypercube sampling of 1000 normally distributed GPD parameter pairs. Note that the fit of the GPD and the uncertainty bounds may not always well capture the observed exceedances (e.g., San Juan; Fig 2A). While we extrapolate estimates for ESL events up to the frequency of the 1000-yr event, we caution in using any estimate of ESL that exceeds four times the length of the observation record (Pugh and Woodworth, 2014). Events that occur with a frequency greater than λ (i.e., the expected number of exceedances of the GPD threshold per year) are outside of the support of the GPD and are modeled with a Gumbel distribution. Other probability mixture model approaches have been proposed that combine a GPD with another distribution (e.g., a Normal distribution; Ghanbari et al, 2019). We do not consider future changes in storm frequency (Walsh et al, 2016), intensity (Sobel et al, 2016), or track (Garner et al, 2017), which could all modify the

GPD parameters. We also do not consider changes in the tide-surge interaction (Schindelegger et al, 2018; Arns et al, 2017) or changes in geomorphology, which can impact storm surge (Familkhalili and Talke, 2016; Talke et al, 2014).

S-1.2 Relative sea level change projections

The other RSLC component contributions are from ocean thermal expansion, glaciers and ice caps, and land-water storage. General circulation model (GCM) output is used to generate the steric and glacial ice melt sea level components for each global mean surface air temperature (GSAT) stabilization scenario. The +2 °C scenario used the GCM outputs specified for the same GSAT scenario in Rasmussen et al (2018) and the +5 °C scenario used GCM outputs from the representative concentration pathway (RCP) 8.5 from Kopp et al (2014). Also accounted for are regional effects such as ocean dynamics (from GCM output), gravitational and rotational effects of ice mass redistribution, glacial isostatic adjustment, and other local vertical land motion factors (e.g., sediment compaction and ground water withdrawal). Probability distributions of local RSLC are produced using 10,000 Latin hypercube samples of each individual sea level component contribution. The probability distributions are truncated at the 99.9th percentile to remove samples that are deemed to be physically implausible (Oppenheimer et al, in press). As noted by Rasmussen et al (2020), both ESL frequencies and allowances are sensitive to truncation selection. More details and limitations to the RSLC projections are provided elsewhere (Kopp et al, 2014; Bamber et al, 2019; Rasmussen et al, 2020).

S-1.3 Exposure analysis

A vertical adjustment was made to the ESLs to reference the same local mean higher high water (MHHW) datum as CoastalDEM. ESLs use tide gauge data for estimating MHHW, while CoastalDEM uses an estimation technique from National Oceanic and Atmospheric Administration's (NOAA) VDatum tool (version 3.7; Parker et al, 2003). This leads to differences in estimates of MHHW for some locations. To convert both data sets to a common vertical reference, an adjustment is made to the tide gauge ESLs to account for differences between the tide gauge estimates and the CoastalDEM ground elevations (adjustments are provided in the supporting data files).

We take a static inundation modeling approach by spatially extrapolating return periods of ESLs, measured at tide gauges, onto the surrounding topography. We map one tide gauge to each city. For cities where there is more than one tide gauge within a 100-km radius (e.g., Willet's Point and the Battery in NYC, Fig. S-6A), the tide gauge with the longest record is used (the tide gauges assigned to each city are listed in the supporting data files). While the height of a given ESL return period may vary within a city, in part due to complicated bathymetry and coastlines, Kulp and Strauss (2017) has shown that ESL population exposure results for the U.S. are generally insensitive to tide gauge assignment within a 100-km radius. In any case, static inundation approaches do not account for complex local geomorphology, local ocean dynamics, and frictional losses as water moves over different land surfaces (e.g., wetlands, beaches, urban areas). More complex hydrodynamic inundation approaches that model the flow of the ocean onto a variety of land surfaces could be used to more accurately estimate local floods for cities across the globe. However, such an approach is out of the scope of this study as our intention is to merely highlight the limitations of physical ESL metrics. Furthermore, we note that hydrodynamic inundation modeling may not necessarily outperform simpler approaches, especially in active tropical cyclone regions (Hunter et al, 2017; Muis et al, 2016, 2017; Wahl et al, 2017), in part due to poor representation of tide-surge interactions (Arns et al, 2020) and short simulation periods that are less likely to produce rare, extreme events found in multi-decadal tide gauge records. For some locations, the height of the 100-yr ESL event can be under-predicted by up to 3 meters compared to tide gauge-derived estimates (supporting information of Muis et al, 2017).

The WorldPop population data are resampled to align with CoastalDEM raster (for more details, see Kulp and Strauss, 2019), integrated over select elevations (-2 to 13 m above MHHW, either 0.25 or 0.5 m increments), and then tabulated according to the satellite-derived urban footprint for each city from Natural Earth (which may differ from the actual administrative boundary; Kelso and Patterson, 2012). We note that Kulp and Strauss (2019) instead uses LandScan population density at 30 arc seconds. Coastal cities are only included in the analysis if there are populations with in the defined boundary at any elevation < 13 m

above local MHHW. Connected components analysis excludes low-elevation inland areas that are not linked to the ocean. Linear interpolation is used between each select elevation to produce a continuous 1-dimensional population exposure profile $D(z)$, where z is the ESL height. We note that z could be a vector to account for spatial differences in ESL height for the same return period within a city and also spatial variation in flood protection.

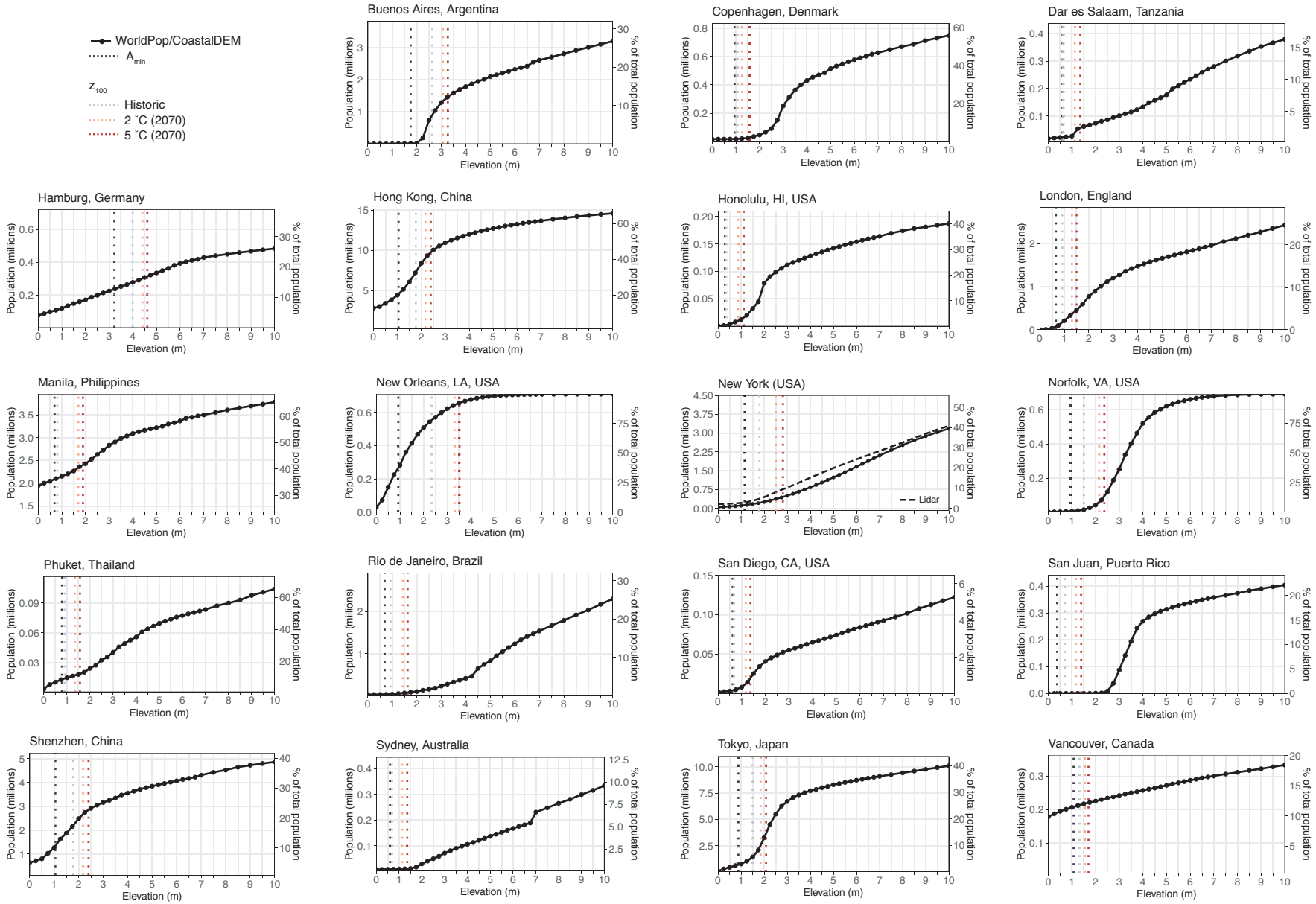

Fig. S-2: Population exposure functions that estimate the total population currently as risk of inundation as a function of ESL height (meters above MHHW) for cities given in Tables 1-4. Filled black circles are population data from the 2010 WorldPop global population database (Tatem, 2017) applied to the elevation surfaces of CoastalDEM (Kulp and Strauss, 2018, 2019). Linear interpolation is used to produce a continuous curve between the WorldPop data (black line). City boundaries are those as defined by Kelso and Patterson (2012) and may differ from actual political boundaries. Populations are assumed to remain constant in time. Denoted is the current level of protection (A_{min}), assumed to be the 10-yr ESL event, the height of the historical 100-yr ESL event (grey), and the expected heights of the 100-yr ESL event under a +2 °C (orange) and +5 °C (red) climate scenario. Also shown for New York City is a population profile generated using a 0.3-m horizontal resolution light detection and ranging (LiDAR)-derived digital elevation model for the City of New York (https://data.cityofnewyork.us/City-Government/1-foot-Digital-Elevation-Model-DEM-/dpc8-z3jc).

S-1.4 Estimating hazard allowances and annual population exposure

While ESL and population exposure AFs are well suited to identify and communicate local coastal flood risks, allowances are perhaps more useful for informing the design of coastal flood defense efforts (e.g., determining optimal levee heights or how high to raise a residence to maintain a given margin of safety; Rasmussen et al, 2020). Following Buchanan et al (2016), we calculate the ESL hazard allowance A that maintains a given annual exceedance probability (AEP) under uncertain RSLC δ, whose uncertainty is given by the PDF, $P(\delta)$,

$$f(z^*) = \int_{\delta} f(z^* - \delta + A(z^*))P(\delta)\,\mathrm{d}\delta, \tag{S-2}$$

where $f(z^*)$ is the current AEP of a given ESL event with height z^* (e.g., the 100-yr event). For a given AEP, the hazard allowance can be interpreted as the horizontal distance between the expected historical and future ESL return curve (Fig. 2A). If δ is known, then $A = \delta$, but if δ is unknown, $A > \delta$ for mathematical reasons given previously (Hunter, 2012; Buchanan et al, 2016; Buchanan et al, 2017). Rasmussen et al (2020) extend the ESL hazard allowance concept to account for the societal impacts of ESL events by employing a simple, time-invariant damage function $D(z)$ that describes the relationship between ESLs and a societal impact (e.g., property damage or population exposure). The damage allowance is the design height of a flood mitigation strategy (e.g., elevation of structures, levee height, necessary coastal retreat) needed to maintain a given integrated exposure metric under RSLC (e.g., current expected annual property damage).

Here we consider the damage (population exposure) allowance needed to maintain the current expected annual population exposure (EAE). The projected EAE under RSLC is given by:

$$EAE = \int_{A_{min}}^{\infty} \int_{\delta} D(z) f(z - \delta) P(\delta)\,\mathrm{d}\delta\,\mathrm{d}z \tag{S-3}$$

where $f(z - \delta)$ is the PDF of ESLs after considering RSLC δ, $P(\delta)$ is the PDF of RSLC δ, $D(z)$ is the populated exposure function (Sec. 2.2), and A_{min} is the height of the assumed current protection level (either no protection, the height of the local 1-yr or 10-yr ESL event; Sec. 2.2).

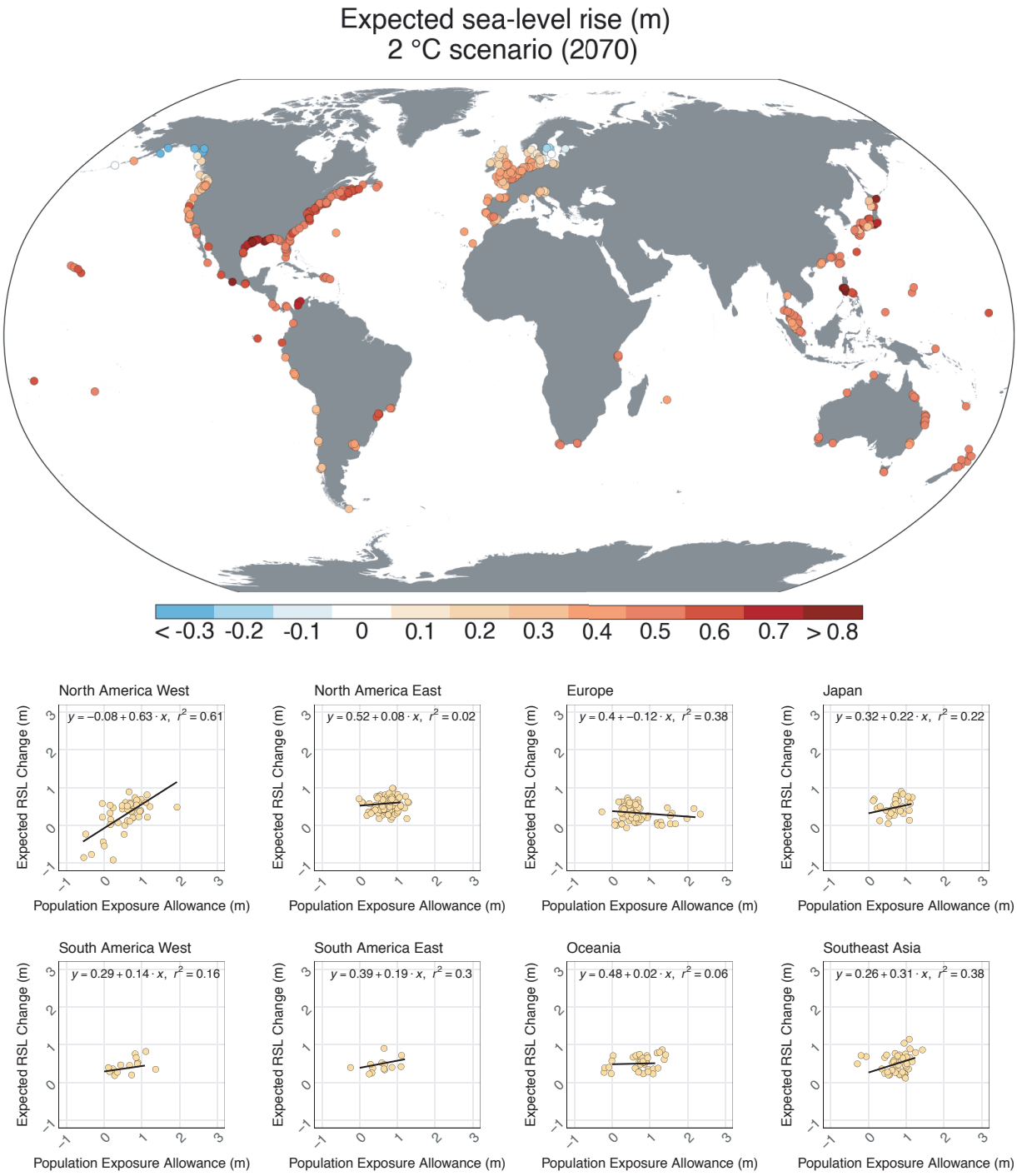

Fig. S-3: **Map:** Expected relative sea level (RSL) change (meters, relative to 1991–2009) for 2070 under a climate scenario where the global mean surface air temperature is stabilized in 2100 at +2 °C (relative to 1850–1900). **Regional scatter plots:** Expected RSL change plotted against population exposure allowances for 2070 that integrate over the entire RSL change probability distribution for the same climate scenario as the map. A list of the cities in each defined region is given in the supporting data files.

New York City	Population		Population Exposure AF			
			2070		2100	
Household income	Total (millions)	% Exposed (Current 100-yr ESL)	2.0 °C	5.0 °C	2.0 °C	5.0 °C
All incomes	8.05	2.8%	1.5 (1.2-1.9)	1.8 (1.3-2.4)	1.8 (1.3-2.6)	2.6 (1.6-4.4)
<$50,000 yr^{-1}	3.54	2.6%	1.5 (1.2-1.9)	1.8 (1.3-2.4)	1.9 (1.3-2.7)	2.7 (1.6-4.7)
$50,000-$100,000 yr^{-1}	2.06	2.9%	1.5 (1.2-1.9)	1.8 (1.3-2.4)	1.8 (1.3-2.6)	2.6 (1.6-4.4)
>$100,000 yr^{-1}	2.32	3.0%	1.5 (1.2-1.9)	1.8 (1.3-2.4)	1.8 (1.3-2.6)	2.5 (1.6-4.2)

Table S-1: Population exposure amplification factors for New York City by household income for 2070 and 2100 under climate scenarios in which global mean surface air temperature is stabilized in 2100 at +2 °C and +5 °C (relative to 1850–1900; Bamber et al, 2019). The expected value and the 5/95 percentile (in parentheses) of the estimate are given for each and reflects the uncertainty in both relative sea level change and the generalized Pareto distribution parameters. Also given are the total populations for each income group and the percent of the group population currently exposed to the 100-yr ESL event. Median household income is given by New York City census tract from the American Community Survey (2014-2018).

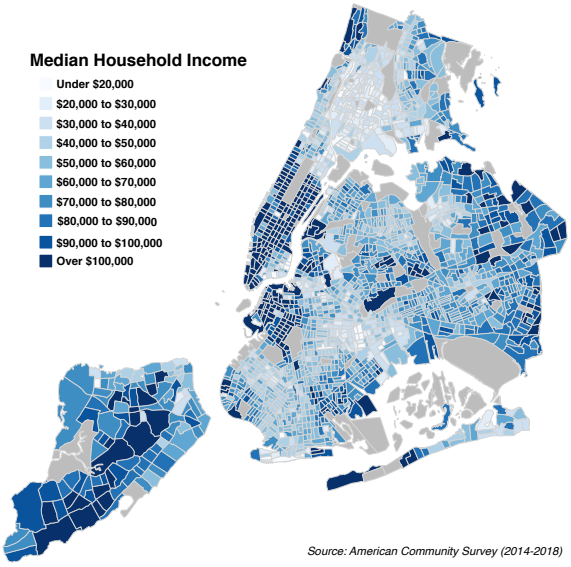

Fig. S-4: Median Household income by New York City census tract from the American Community Survey (2014-2018).

New York City		Property Damage AF			
		2070		2100	
	Current 100-yr ESL	2.0 °C	5.0 °C	2.0 °C	5.0 °C
Property Damage	$4 billion ($2-$7 billion)	2.0 (1.4-2.9)	2.6 (1.6-3.9)	2.7 (1.5-4.3)	4.2 (2.0-7.8)

Table S-2: Property damage amplification factors for New York City for 2070 and 2100 under climate scenarios in which global mean surface air temperature is stabilized in 2100 at +2 °C and +5 °C (relative to 1850–1900; Bamber et al, 2019). The expected value and the 5/95 percentile (in parentheses) of the estimate are given for each and reflects the uncertainty in both relative sea level change and the generalized Pareto distribution (GPD) parameters. Also given is the current expected damage from the 100-yr ESL event with the 5/95 percentile estimates in parentheses (samples uncertainty in the GPD parameters only). Monetary amounts assume constant 2017 US$. The methods for calculating the damage function are given in Rasmussen et al (2020).

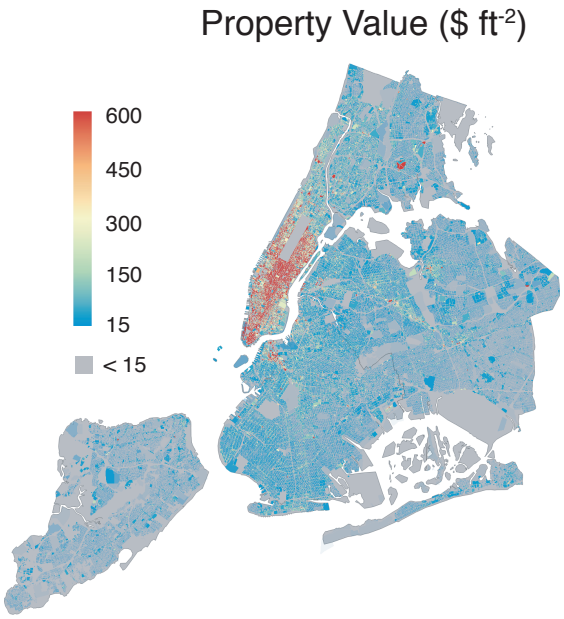

Fig. S-5: The estimated density of property for New York City (excludes land value) given as the tax assessed building value per square foot of building lot area (2017 US$ ft^{-2}). Data are from the NYC Department of City Planning (NYC Planning, 2018).

2.0 °C	2010	2070		2100	
	Population (thousands)	Population (thousands)	Pop Exposure AF	Population (thousands)	Pop Exposure AF
Lidar	399 (293-564)	607 (488-745)	1.5 (1.2-1.9)	708 (518-938)	1.8 (1.3-2.4)
CoastalDEM	229 (168-324)	351 (280-440)	1.5 (1.2-1.9)	421 (297-596)	1.8 (1.3-2.6)

Table S-3: Estimated total population exposure and amplification factors for the 100-yr extreme sea level (ESL) event for New York City using 1) a 0.3-m horizontal resolution light detection and ranging (LiDAR)-derived digital elevation model for the City of New York (https://data.cityofnewyork.us/City-Government/1-foot-Digital-Elevation-Model-DEM-/dpc8-z3jc) and 2) CoastalDEM. Future projections assume a climate scenarios in which global mean surface air temperature is stabilized in 2100 at +2 °C (relative to 1850–1900; Bamber et al, 2019).

5.0 °C	2010	2070		2100	
	Population (thousands)	Population (thousands)	Pop Exposure AF	Population (thousands)	Pop Exposure AF
Lidar	399 (293-564)	687 (529-880)	1.7 (1.3-2.2)	917 (617-1,398)	2.3 (1.5-3.5)
CoastalDEM	229 (168-324)	405 (303-548)	1.8 (1.3-2.4)	589 (355-1,010)	2.6 (1.6-4.4)

Table S-4: As for Table S-3, but for a climate scenarios in which global mean surface air temperature is stabilized in 2100 at +5 °C (relative to 1850–1900; Bamber et al, 2019).

					2.0 °C								
		2010 EAE (millions)			2050 EAE AF			2070 EAE AF			2100 EAE AF		
City	Population (millions)	None	1-yr	10-yr	None	1-yr	10-yr	None	1-yr	10-yr	None	1-yr	10-yr
Shenzhen, China	12.52	1.07	0.70	0.70	1.3	2.0	2.0	1.6	2.5	2.5	2.3	3.5	3.5
Vancouver, Canada	1.81	0.20	0.13	0.13	1.0	1.6	1.6	1.0	1.7	1.7	1.1	1.8	1.8
New York, USA	12.52	0.22	0.15	0.15	1.4	2.1	2.1	1.8	2.6	2.6	2.8	4.1	4.1
London, UK	9.88	0.04	0.03	0.03	3.0	3.6	3.6	5.0	5.9	5.9	9.9	11.7	11.6
Buenos Aires, Argentina	11.98	0.03	0.03	0.03	2.0	2.1	2.1	3.4	3.5	3.5	11.7	12.1	12.2
San Diego, USA	2.32	<0.01	<0.01	<0.01	2.4	4.3	4.3	5.2	9.1	9.1	12.5	21.8	21.8
Rio de Janeiro, Brazil	9.11	0.03	0.02	0.02	1.3	2.2	2.2	2.0	3.3	3.3	4.1	6.7	6.7
Hong Kong, China	22.23	3.99	2.53	2.53	1.2	1.9	1.9	1.4	2.2	2.2	2.1	3.3	3.3
Manila, Philippines	5.78	2.06	1.24	1.24	1.1	1.8	1.8	1.1	1.9	1.9	1.3	2.2	2.2
Copenhagen, Denmark	1.34	0.02	0.01	0.01	2.3	3.8	3.8	4.9	7.8	7.8	15.1	24.4	24.4
Dar es Salaam, Tanzania	2.32	0.02	0.01	0.01	1.2	2.3	2.3	2.2	3.9	3.9	3.3	5.9	5.9
Sydney, Australia	3.48	0.01	<0.01	<0.01	1.1	1.8	1.8	1.2	2.0	2.0	3.2	5.2	5.2
Phuket, Thailand	0.16	0.01	0.01	0.01	2.0	2.3	2.3	2.3	3.4	2.3	3.4	3.4	3.4
Tokyo, Japan	25.34	0.55	0.38	0.38	1.4	2.1	2.1	2.0	2.9	2.9	5.9	8.7	8.7
New Orleans, USA	0.71	0.17	0.13	0.13	2.2	3.0	3.0	2.8	3.7	3.7	3.6	4.7	4.7
Norfolk, USA	0.69	<0.01	<0.01	<0.01	2.0	2.7	6.9	3.4	4.7	13.7	13.9	19.0	55.5
San Juan, Puerto Rico	1.82	<0.01	<0.01	<0.01	2.5	2.6	2.7	3.0	3.1	3.3	16.6	17.3	18.3

Table S-5: expected annual population exposure (EAE; millions) under different assumptions of existing coastal flood protection (no protection and protection against the 1-yr and 10-yr events) and amplification factors (AFs) for the EAE for 2050, 2070, and 2100 under the same coastal flood protection assumptions and under a climate scenario in which global mean surface air temperature is stabilized in 2100 at +2 °C (relative to 1850–1900; Bamber et al, 2019).

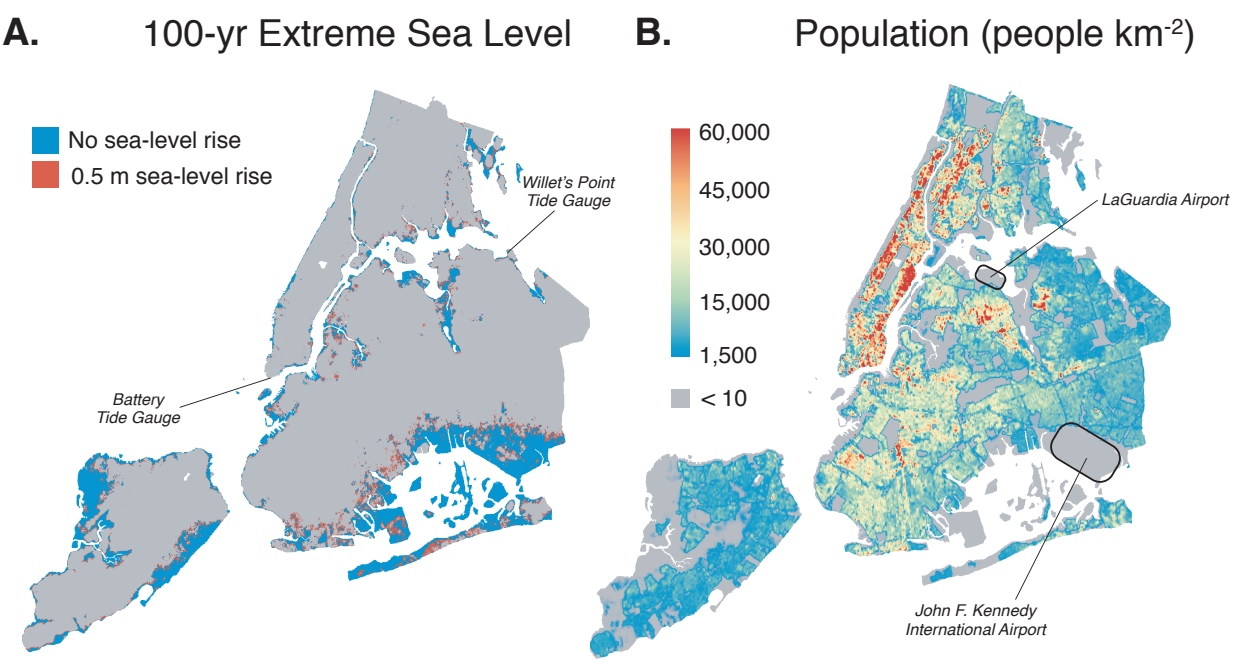

Fig. S-6: **A.** The estimated spatial flood extent for New York City as a result of the 100-yr extreme sea level (ESL) event under 1991–2009 mean sea level (blue) and with 0.5 m of sea-level rise (red; extent above 1991–2009 levels). The "bathtub" approach (Sec. 2.2) is used to model flood inundation using the height of the current and projected future 100-yr ESL event at a tide gauge located at the Battery. Topography data are CoastalDEM (Kulp and Strauss, 2018). **B.** The estimated population density (people km^{-2}) for New York City from the 2010 WorldPop global population database (Tatem, 2017). Highlighted are the locations of John F. Kennedy International and LaGuardia Airports, critical infrastructure at risk that is not represented using population data.